Title: Impact of redox fluctuations on the spatial distribution of the microbial community in a forest soil: A lysimeter experiment

Simiao Wang[a], Filippo Miele[b], Paolo Benettin[b,c], Mitra Asadollahi[b], Jacopo Pasqualini[d] , Manon Frutschi[a], Pierre Rossi[e], Nicolas Jacquemin[a], Andrea Rinaldo[b], Rizlan Bernier-Latmani[a]

[a] Environmental Microbiology Laboratory, École polytechnique fédérale de Lausanne, Switzerland
[b] Ecohydrology Laboratory, École polytechnique fédérale de Lausanne, Switzerland
[c] Institute of Earth Surface Dynamics, Université de Lausanne, Switzerland
[d] Laboratory of Interdisciplinary Physics, University of Padua, Italy
[e] Central Environmental Laboratory, École polytechnique fédérale de Lausanne, Switzerland

Corresponding author: Rizlan Bernier-Latmani
Email Address:
Simiao Wang: simiao.wang@epfl.ch
Filippo Miele: filippo.miele@epfl.ch
Paolo Benettin: paolo.benettin@epfl.ch
Mitra Asadollahi: ma4451@columbia.edu
Jacopo Pasqualini: jacopo.pasqualini@studenti.unipd.it
Manon Frutschi: manon.frutschi@epfl.ch
Pierre Rossi: pierre.rossi@epfl.ch
Nicolas Jacquemin: nicolas.jacquemin@epfl.ch
Andrea Rinaldo: andrea.rinaldo@epfl.ch
Rizlan Bernier-Latmani: rizlan.bernier-latmani@epfl.ch

Abstract:

The soil microbial community is structured by several factors including environmental conditions such as varying water content, dissolved oxygen, and redox potential. Here, we experimentally investigate the impact of the redox regimes, i.e., oxic, fluctuating, or anoxic conditions, on the microbial community composition and probe the widespread hypothesis that the diversity of the redox fluctuating layer is greater than that of the zones with static redox conditions. A 50-cm homogenized soil column was subjected to realistic intermittent artificial precipitation for 3 months and the hydrological and geochemical parameters (redox potential, pH, dissolved oxygen, soil moisture, matric potential, chemical speciation) measured as a function of time and depth. The change in microbial community over the 3-month experiment was distinct in the three redox zones. The oxic zone exhibited increased biomass and the highest diversity, the redox fluctuation zone exhibited less growth and diversity, and the anoxic zone was characterized by little change in biomass and minimal change in diversity. Interestingly, the redox fluctuation zone and anoxic zone microbiomes most resembled that of the initial soil. Rather than the redox potential alone, the vertical DOC gradients were found to dominate the compositional trajectory of the microbiome. Additionally, this work validated a recently developed spatially explicit biogeochemical model with both geochemical and microbial data and revealed the horizontal and vertical characteristics of microbial community diversity under varying hydrological regimes.

1. Introduction

Globally, soil stores ~2,200 Pg of carbon (C) (including 1,500 Pg of organic C) and 136 Pg of nitrogen (N) in its top 1 m layer. It represents the largest pool of terrestrial C and N on the planet and acts both as a source and a sink for greenhouse gases (GHG) such as carbon dioxide (CO_2), methane (CH_4), and nitrous oxide (N_2O) (Batjes, 1996; W. Kutsch et al., 2009; Oertel et al., 2016), with soil CH_4 and N_2O emissions almost exclusively of biological origin (Conrad, 2009; Meixner & Yang, 2006; Schaefer et al., 2016; Serrano-Silva et al., 2014; Syakila & Kroeze, 2011). The fluxes of CH_4 and N_2O depend on the relative contribution of oxidative and reductive microbial processes within the soil, which are tightly controlled by redox potential (Ambus et al., 2006; Bremner, 1997; Grunwald et al., 2012; Hungate & Koch, 2003). Hence, while microbial activity is a driver for GHG production, redox potential (E_h) is a major controlling factor for soil microbial metabolism.

In natural soils, aerobic respiration is expected to take place at E_h values of 800 mV and denitrification at 550 mV, while methanogenesis requires redox potentials of -200 mV (Hirano et al., 2013; Masscheleyn et al., 1993; Reeburgh, 1983; Wang et al., 2018). In turn, the local availability of electron donors and acceptors is largely forced by hydrological dynamics occurring within the soil: the degree of soil saturation limits oxygen availability (Haberer et al., 2012; Liptzin et al., 2011) and, under increasingly saturated conditions, O_2 becomes limiting allowing the establishment of reductive metabolisms such as iron or sulfate reduction. Thus, soil redox potential values can exhibit rapid and large variations in response to dynamic hydrological conditions (Zhang & Furman, 2021).

Furthermore, soil redox is also expected to shape the microbial community by providing environments that are more favorable for some taxa rather than others. Drenovsky et al. (2004) proved the deterministic role of soil moisture content and organic carbon availability in soil microbial community compositions with phospholipid fatty acid analysis. Ma et al. (2015) also pointed out that wet soil conditions favor Gram-positive bacteria while dry soil conditions favor Gram-negative bacteria and fungi. Both experiments showed that flooding conditions with low O_2 levels and E_h would select facultative and obligate anaerobes while dry soil conditions with high O_2 levels and E_h would select obligate aerobes (Drenovsky et al., 2004; Ma et al., 2015). Moreover, in the soil incubation experiment conducted by DeAngelis et al. in 2010, over 200 taxa were shown to be more active under fluctuating redox conditions and only 3 taxa showed higher activity under static anoxic conditions.

Zones characterized by dynamic oxic/anoxic transitions have often been suggested as hotspots for microbial activity (e.g., DeAngelis et al., 2010a; Gordon et al., 2008; Hutchinson, 1961; Miele et al., 2023; Pett-Ridge & Firestone, 2005). This observation has been attributed to the spatiotemporal soil heterogeneity, which allows a wide diversity of microorganisms to coexist (Degens et al., 2001; Fierer et al., 2003; Peralta et al., 2014; Rühle et al., 2015). However, other studies suggested that the microbial community structure did not change significantly with drying-rewetting cycles due to the resilience of the community to significant changes in water availability (Rezanezhad et al., 2014; Šťovíček et al., 2017; Zhou et al., 2016). In addition, the microbial community within oxic (static) environments evidenced the highest diversity due to the fueling of the metabolism of a large diversity of aerobes and facultative aerobes (Song et al., 2008). In contrast, the community in anoxic (static) environments typically exhibits the lowest diversity (Pett-Ridge & Firestone, 2005).

Many of the abovementioned studies were conducted with soil incubation experiments in jars or bottles (DeAngelis et al., 2010; Peralta et al., 2013; Pett-Ridge & Firestone, 2005; Xiang et al., 2008; Yu et al., 2007), which do not allow for the spatially resolved characterization of the impact of E_h and moisture dynamics on the microbial community. Natural environments are known to be subjected to variable rainfall inputs that cause water and oxygen availability to change with depth. Instead of artificially establishing static or dynamic redox conditions in discontinuous systems, it is more representative to study the impact of a fluctuating water table on microbial diversity using a

soil column. Rühle et al. (2015) investigated microbial activity in soil columns by comparing two soil columns with a static water table to columns with a fluctuating water table. They found that the microbial community abundance decreased with depth but that the bacterial diversity was not significantly different between the two columns nor along either column. Yet, they identified specific taxa present only in the column with the fluctuating water table, especially in the fluctuating zones. Their results evidence the complexity of the relationship between local hydrologic fluctuations and soil microbial community diversity.

While laboratory and field experiments deliver insights into soil biogeochemical processes, biogeochemical models are a powerful tool to decipher and predict the impact of biotic and abiotic variables on nutrient dynamics (Berardi et al., 2020; Bonan, 2019; Tecon & Or, 2017). However, most models do not include spatial resolution of hydrological processes and they are often not validated on real-world data (Calabrese & Porporato, 2019; Manzoni & Porporato, 2007; Rubol et al., 2013).

Here, we ran a lab-scale soil column experiment under controlled rainfall conditions to investigate the impact of water table and redox potential fluctuations on the spatial distribution and diversity of the soil microbiome. We collected and homogenized soils from a forest near Lausanne (CH) and used them to fill a 50-cm long and 30-cm diameter lysimeter. We probed the spatial distribution of the initially uniform microbial community after three months of intermittent precipitation mimicking realistic daily precipitation at-a-point (Rodriguez-Iturbe et al., 1987, 1999) and measured the temporal variation in potential drivers for the change in microbial composition, i.e., environmental factors such as dissolved oxygen (DO), soil moisture content, and nutrient availability. By characterizing the spatial distribution of the microbial community at the beginning and at the end of the experiment, its compositional trajectory was reconstructed under variable redox conditions: oxic, fluctuating redox and anoxic. Finally, we used the recently developed spatially explicit modeling framework by Miele et al. (2023), validated on our experimental data, to reconstruct the microbial activity within the soil as a function of depth. Cross-comparison of the changes in the microbial community and the predicted microbial metabolisms provided an independent validation of the accuracy and limitation of the model. Through these results, we address the following research questions:

1) What are the dominant biogeochemical processes within a soil column under controlled dynamic hydrologic conditions?

2) What is the spatio-temporal evolution of microbial communities under distinct redox conditions?

3) What is the effect of redox fluctuations on soil microbial biodiversity?

While our results are based on a specific lab-scale experimental setup, the rainfall regime that we imposed allows us to target general trends in relation to hydrologic conditions, redox dynamics, and microbial responses in soils.

2. Materials and methods

2.1 Experimental set-up

A weighted soil column (usually called weighed lysimeter or simply lysimeter, **Figure 1**) was used to study a forest soil under controlled conditions. The lysimeter is a 60-cm high and a 30-cm diameter PVC column placed on a weighting platform. The bottom of the column is sealed with a porous plate. The porewater that drains through the porous plate by gravity is directed to a small pipe through a funnel. The pipe was bent upward to function as a siphon and to control the water table level. The expected water table level was between 28 and 36 cm below the soil surface, however, at times, it was impacted by clogging of the lysimeter bottom, precluding drainage. The lysimeter was filled with 50 cm of soil (see next section). Suction cups and various probes were

inserted into the lysimeter at different depths (detailed information in **Figures 1b** and **1c**) to allow the collection of porewater samples at various depths (suction cups) and continuous measurement of soil conditions including redox potential (E_h), pH values, soil moisture, water tension (matric potential), and dissolved oxygen (DO). A gas chamber with two valves was fixed to the top of the lysimeter for soil gas emission analysis. One was connected to a vacuum pump and the other was open to the atmosphere to allow gas exchange between gas chamber and ambient air. A sprinkler was installed at the top of the gas chamber and connected to an irrigation pump to control the precipitation applied to the lysimeter.

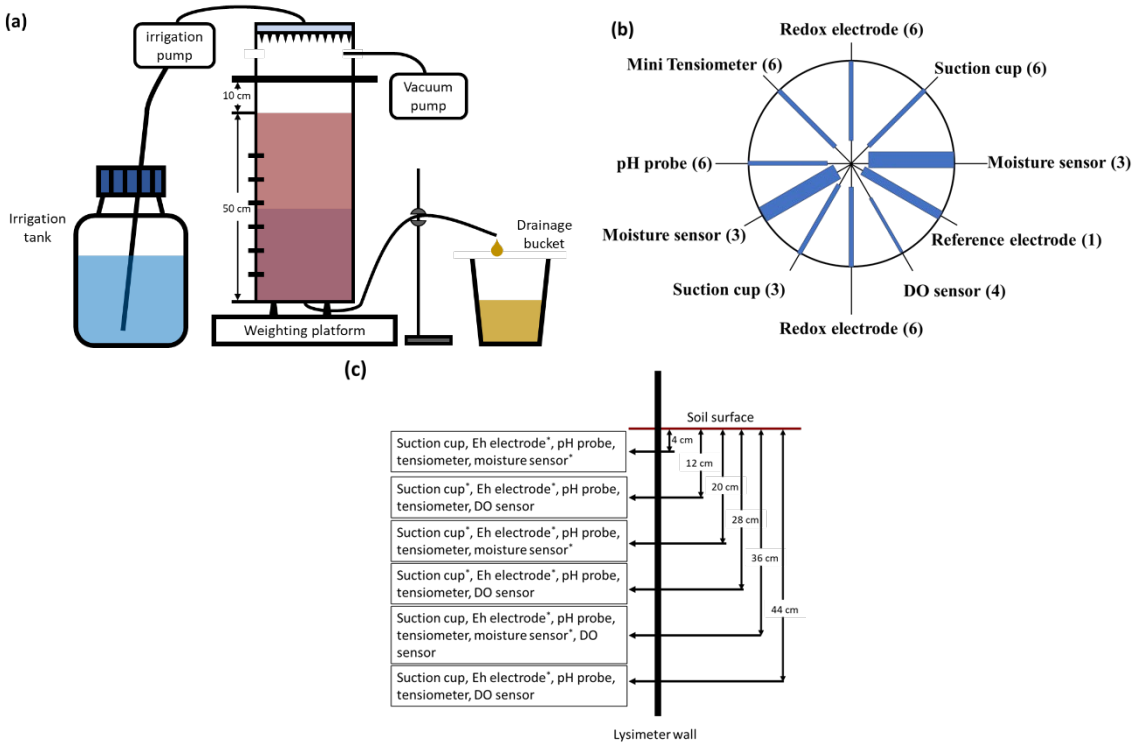

Figure 1 Illustration of the experiment setup. (a) schematic sketch of the lysimeter's setup; (b) top-down view of probes and suction cups within the lysimeter. The numbers in parentheses refer to the number of probes/suction cups in a vertical column; (c) vertical sketch of probes and suction cups within the lysimeter, * refers to duplicate probes/suction cups at the same depth.

2.2 Soil preparation and packing

Soil from a beech/pine mixed forest in Lausanne (Switzerland), that was characterized by the SwissMEX project, was collected on September 2021 to a depth of 20 cm depth (Mittelbach H., 2011). Visible plant material was removed from the soil which was dried at 40 °C for two days, then ground and sieved to 2 mm (Huang et al., 2011). The soil was finally homogenized by mixing all soil batches in a clean cement mixer. Some soil was further sieved to remove particles < 50 µm to produce coarse soil that was used to pack the bottom 5 cm of the soil column (4 kg of soil) to preclude bottom plate clogging (this represents "initial bottom" soil, 45-50 cm from the top of the lysimeter). The rest of the column was packed using sieved soil via a dry-packing method: 4.2 kg of soil was added at a time into the lysimeter, compacted with a wooden compactor to 5cm per layer. To avoid discontinuity between layers, the soil surface was scraped before the addition of a new layer. This process was repeated until the soil column reached 40 cm (this represents "initial middle" soil, 10-45 cm from the top of the lysimeter). Dry leaves were collected at the same site and had a total organic carbon (TOC) around 42.5% by mass. They were blended and mixed with sieved soil (native TOC around 2.6% by mass) and the mixture, containing 18% TOC by mass, was packed in the top 10 cm of the soil column (2.25 kg of soil-leaf mixture per 5 cm) and served as an organic

carbon source for the soil column (this represents "initial top" soil 0-10 cm from the top of the lysimeter). Artificial rainwater (recipe in **Table 1**) was applied from the top of the lysimeter via the sprinkling head. The soil column was then flushed with artificial rainwater from the bottom of the lysimeter to saturate the soil column, and subsequently drained from the bottom. This process was repeated 5 times for 10-50cm depth part of the soil column and twice for the whole column to remove excess labile organic carbon and potentially entrapped air. At the end of the last drainage, the drainage tube was lifted to the appropriate elevation to function as a siphon and control the water table level at 28-36 cm below the soil surface.

Compound	Concentration (µM)
Ca^{2+}	54.49
Mg^{2+}	4.79
Na^{+}	7.24
K^{+}	2.37
NO_3^{-}	7.24
SO_4^{2-}	4.79
Cl^{-}	2.37
HCO_3^{-}	108.98

Table 1 Artificial rainwater recipe adapted from an unpublished investigation by Jana von Freyberg

2.3 Experiment description and sample collection

Artificial rainwater was applied to the lysimeter over three months via an irrigation pump programmed to deliver a computer-generated rainfall timeseries (**Figure 2**). The rainfall distribution follows a Marked Poisson process, which reproduces closely real-world precipitation patterns (Rodriguez-Iturbe et al., 1987). The parameters of the Poisson process are the overall precipitation amount (408 mm) and mean inter-arrival time (3 days). These were selected based on average annual precipitation data for Switzerland from 1991 to 2020 (Federal Office of Meteorology and Climatology MeteoSwiss, 2021).

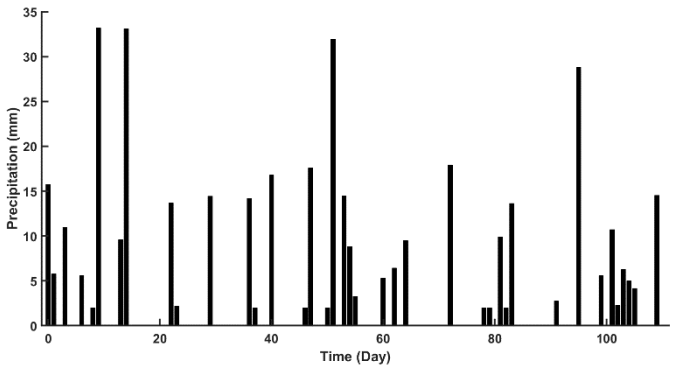

Figure 2: Experimental daily rainfall timeseries generated following a Marked Poisson process (Rodriguez-Iturbe et al., 1987) based on precipitation statistics from Switzerland from 1991 to 2020

During the experiment, 10 mL sealed serum bottles filled with N_2 were used to collect porewater samples every 3-4 days. The serum bottles were connected both to the suction cup and to a vacuum pump set at ~ -0.8 bar. Between 2 and 6 mL of porewater were collected from each suction cup. After sample collection, serum bottles were moved to an N_2-filled glovebox (MBraun LABstar Pro, Germany) and porewater filtered through 0.22 µm polyethersulfone filters and re-distributed into five 1.5 mL polypropylene tubes. Three of the subsamples containing 0.4 mL porewater were stabilized with 0.4 mL of 2 M hydrochloric acid (HCl), 0.4 mL of 1% nitric acid (HNO_3), or 0.1 mL of

5% zinc acetate ($Zn(Ac)_2$) respectively for subsequent quantification of dissolved ferrous iron (Fe(II)), manganese ion (Mn^{2+}), and sulfide (HS^-). The remaining sample was used for analysis of dissolved organic carbon (DOC) and anions and cations, such as nitrate (NO_3^-), nitrite (NO_2^-), sulfate (SO_4^{2-}) and ammonium (NH_4^+). After stabilization, samples were moved out from the glovebox and stored at 4 °C until analysis. Simultaneously, gas samples were also collected and analyzed for N_2O and CH_4 emissions as well as N_2O site-preference (SP) values (see Supplementary Information for details).

At the end of the experiment, a 3-cm-diameter auger was used to collect soil cores along the entire depth of the soil column at 5 positions in the lysimeter, a central core (CC) and 4 peripheral (side) cores (SC) (**Figure S1**). Each soil core was cut into segments 4 cm-thick and each segment was transferred to a 50-mL sterile tube (Falcon® 50 mL High Clarity Conical Centrifuge Tubes, USA) and stored at -80 °C. These soil samples were used for soil microbial community analysis.

2.4 Sample analysis

Concentrations of NO_3^-, NO_2^-, SO_4^{2-} and NH_4^+ were quantified by ion chromatography (Thermo Scientific™ Dionex™ ICS-6000 Capillary HPIC™) while DOC was quantified with a TOC analyzer (Elementar Vario TOC Cube, Germany). Concentrations of Fe(II), HS^- and Mn^{2+} were quantified colorimetrically using a UV-vis spectrophotometer (Shimadzu UV-2501PC UV-vis recording spectrophotometer, Japan) (Supplementary Information for details).

Soil samples (200-300 mg) were amended with 50 µL of ZymoBIOMICS™ Spike-in Control I (High Microbial Load), which contained 5 x 10^7 cells of *Imtechella halotolerans* (Gram-negative) and *Allobacillus halotolerans* (Gram-positive), as well as 5 x 10^7 cells of *Pediococcus acidilactici* (Gram-positive) as internal controls to check for biases in DNA extraction. DNA was extracted from soil using the DNeasy PowerSoil Pro Kit and a QIAcube Automated Robotic DNA/RNA Purification System (both QIAGEN, USA). Extracted DNA samples were amplified with PacBio bacterial full-length 16S rRNA gene with barcoded primers in peqSTAR Thermal Cycler (Peqlab, Germany) and sequenced with the PacBio Sequel II system. The 16S rRNA copies were quantified by qPCR performed with the Magnetic Induction Cycler qPCR machine (BioMolecular Systems, Australia) with the calibration curve based on known concentrations of *E. coli*. By combining the relative abundance of *P. acidilactici, I. halotolerans* and *A. halotolerans* obtained from sequencing results and the absolute abundance of 16S rRNA gene copies obtained from qPCR, estimations can be provided for the extracted copies of *P. acidilactici*, *I. halotolerans* and *A. halotolerans*. This data is used to prove that there is no systematic bias in DNA extraction among samples collected at different depths of the lysimeter (**Figure S2**).

γ-diversity broadly describes the number of species in a large area (Andermann et al., 2022) while β-diversity describes the difference in populations (i.e., specific species) across sites. Calculation of β diversity varies across studies (Andermann et al., 2022). In this experiment, we use the β diversity calculation as defined by Sorensen (1948) and modified by Baselga (2010) for multiple-site dissimilarity (β_{SOR}). It is defined according to the following equations for site *j* compared with *N* neighboring sites (*i*). *j* was defined as *N+1*.

$$\beta_{SOR} = \frac{[\sum_{i<j} min(b_{ij},b_{ji})]+[\sum_{i<j} max(b_{ij},b_{ji})]}{2[\sum_i S_i - S_T]+[\sum_{i<j} min(b_{ij},b_{ji})]+[\sum_{i<j} max(b_{ij},b_{ji})]} \qquad \textbf{\textit{Equation (1)}}$$

Where
b_{ij} = number of species only present in site *i*
b_{ji} = number of species only present in site *j*
S_i = Total number of species in site *i*
S_T = Total number of species in all sites combined

2.5 Spatially Explicit Compartment Model for Reactive Transport

To interpret the vertical profile of the experimental data, we follow the approach by Miele et al. (2023) to model the soil column as a one-dimensional layered system, where each simulated soil layer is selected to match the position of redox probes in our experimental lysimeters. Thus, the column is subdivided into five layers of 8cm thickness each and one layer of 10cm. Following Miele et al. (2023), the microbial activity is described by biomass (BM, expressed in cells/kg of dry soil) and the kinetics of microbially mediated reactions. Specifically, any rate is composed by multiplying BM concentration by the concentration of both the electron donor (e.g., DOC or NH_4^+) and the electron acceptor, to account for the corresponding processes. The DOC dynamics are regulated by two positive terms that encode both soil organic carbon (SOC) conversion (assumed to be constant) and biomass decay rate and a negative contribution due to the use of OC as an electron donor in the aerobic and anaerobic metabolisms involved. As oxygen diffusion in water is negligible, O_2 supply through all the layers is mainly driven by air-water saturation cycling. O_2 diffusion by concentration gradient into the liquid phase is only considered in the first layer, due to the open-air exposure of the surface layer, through a modified Henry's law that includes temperature effects and soil volumetric air-filled porosity effects.

Further, while oxygen is the dominant electron acceptors in aerobic condition, anaerobic metabolisms that hierarchically involve NO_3^-, Mn(IV), Fe(III) and SO_4^{2-} reduction are subsequently considered according to the common redox ladder order (Zhang & Furman, 2021). This is achieved further by multiplying each kinetic rate by a Monod-type limiting factor that inhibits the reduction of a specific electron acceptors unless all the more energetically favored others are depleted.

Finally, the pivotal role of soil moisture in shaping aerobic and anaerobic respiration is expressed by the moisture functions where soil field capacity (s_{fc}) defines a critical threshold above which aerobic respiration is inhibited.

Moreover, due to the soil's structural heterogeneity, expressed by micro fractures, preferential flow paths, and the soil-lysimeter interface, transport is described in terms of internal flux exchanges between connected layers. This is achieved by assuming that each layer acts as a compartment where water discharge is expressed by a power function (Laio et al., 2001; Manzoni & Porporato, 2007) and each layer's outflow is partitioned to subcomponent fluxes among all the other subsequent layers.

The spatio-temporal pattern of redox potential at each of the 6 layers are determined by the Nernst equation (Miele et al., 2023; Rodríguez-Escales et al., 2020), that combines the time-variable concentration of each redox couple:

$$E_h = E_h^0 - \frac{RT}{n_e F} \ln \frac{[B]^b [D]^d}{[A]^a [C]^c} \qquad \textbf{\textit{Equation (2)}}$$

for a generic redox reaction such as:

$$aA + cC \rightarrow bB + dD \qquad \textbf{\textit{Equation (3)}}$$

By normalizing at each time point the virtual electron flux exchanged by each redox reaction, it is possible to reconstruct the relative dominance of each metabolism.

3. Results

3.1 Spatial and temporal response of soil physiochemical parameters to precipitation

The lysimeter was divided into 6 layers where each includes probes and microbial community analysis at or near their midpoint (layer 1: 0-8 cm, referred to as the 4-cm layer; layer 2: 8-16 cm, 12-cm layer; layer 3: 16-24 cm, 20-cm layer; layer 4: 24-32 cm, 28-cm layer; layer 5: 32-40 cm, 36-cm layer; layer 6: 40-50 cm, 44-cm layer). The spatial-temporal variation of soil volumetric water content (VWC), water table level (based on matric potential), Eh, and DO are plotted as a function of time and space in **Figure 3 & S3**.

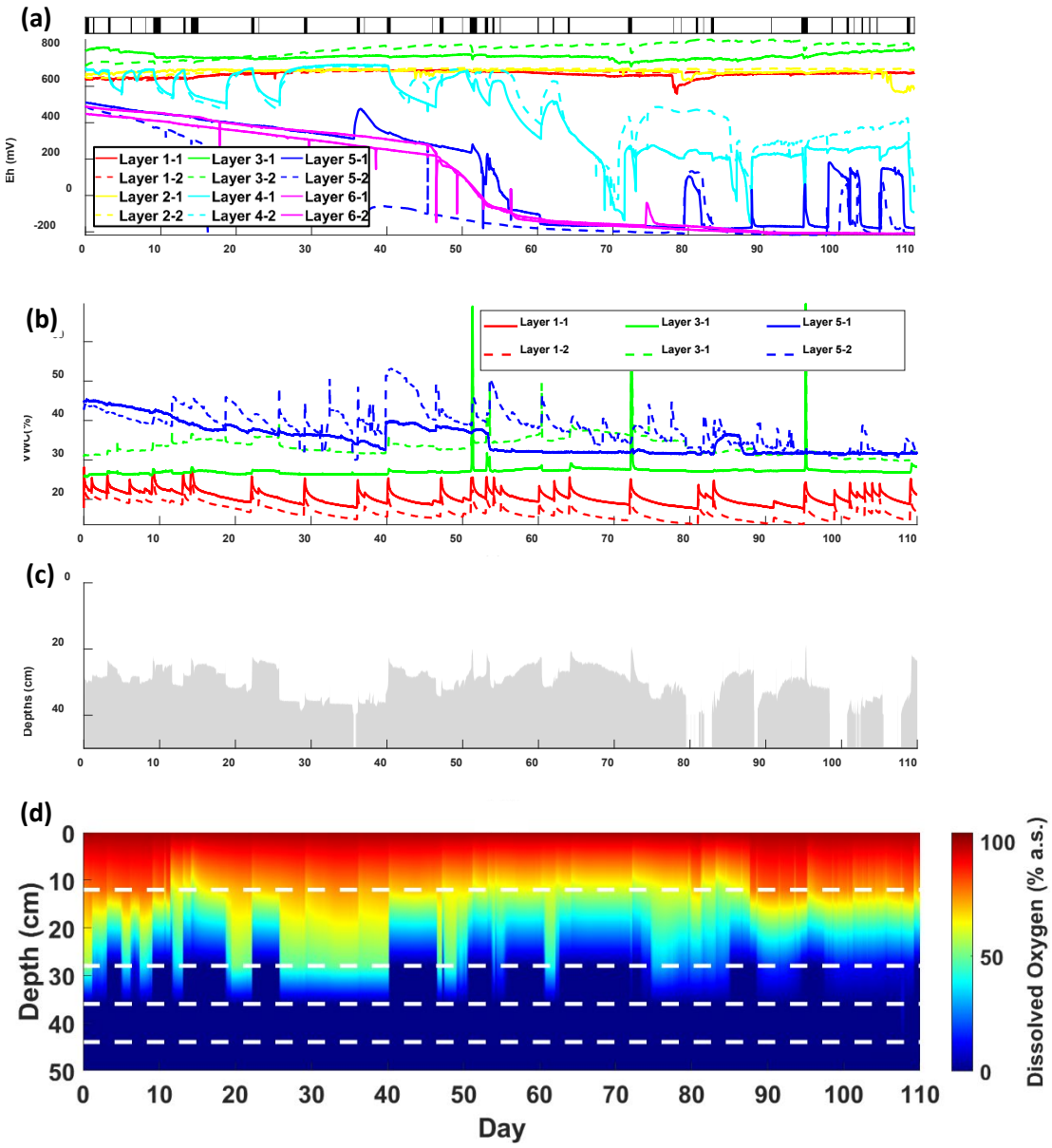

Figure 3: Spatial and temporal response of soil physical and chemical parameters to precipitation events. The narrow bar plots at the top represents precipitation events with the bar width proportional to the volume delivered for individual precipitation events. Layer X-1 & X-2 refers to measurements from duplicate probes at the same depth. (a) Soil redox potential values measured at 6 depths every 5 minutes with duplicate redox electrodes at each depth normalized to the Standard Hydrogen reference Electrode (SHE). (b) Soil volumetric water content (in %) measured at 3 depths every 5 minutes with duplicate moisture sensors at each depth. (c) Estimated water table depth based on matric potential measured by a tensiometer at 36 cm depth. Missing values of the estimation suggest a water table depth below 40 cm depth due to

tensiometer readings at 36 cm depth becoming unreliable. (d) Dissolved oxygen concentrations (as % of air saturation) heatmap developed based on DO sensors at 4 depths (indicated by white dotted lines).

Soil E_h values exhibit three distinct responses, varying with depth (**Figure 3a and S3**). First, E_h values measured by the redox electrodes in the top three layers (4-cm, 12-cm, 20-cm) remained relatively constant between 600 and 800 mV throughout the whole experiment. However, E_h values measured in layer 4 (28-cm) fluctuated between 300 and 700 mV in response to precipitation events until day 55. From day 55 to day 110, fluctuation in response to precipitation events continues, but the range of E_h values shifted down to between -110 mV to 500 mV. Finally, in layers 5&6 (36- and 44-cm), E_h values continuously decreased from 500mV to -200mV with a sharp decrease between day 50 and 60. E_h values in layer 5 also fluctuated in response to precipitation events, similarly to the layer 4 case, from day 80 to day 110.

As expected, soil moisture content, measured as volumetric water content (VWC), was directly impacted by precipitation events (**Figure 3b**). In general, VWC increases with depth, likely due to downward porewater advection, as well as evaporation at the soil surface. An increase in VWC was observed at all depths during or after the precipitation event, followed by a gradual decrease to a stable value in the absence of rainfall. With each precipitation event, the magnitude of VWC increases transiently in layers 1&3. In contrast, the soil water content in layer 5 is generally higher than in layers 1&3, throughout the experiment, due to the accumulation of water at that depth.

The depth of the water table was estimated based on readings from a tensiometer at 36 cm (layer 5) (**Figure 3c**). This tensiometer remained below the water table for most of the experiment. Water table level changes corresponded to precipitation events and fluctuated mainly between 25 and 40 cm (within layers 4&5). DO concentrations were measured with DO sensors in layer 2 & layers 4-6 (**Figure 3d**). DO concentrations in layer 2 remained close to atmospheric level throughout the experiment, while DO concentrations in layers 5&6 remained close to 0. in layer 4, DO concentrations fluctuated between ~60% air saturation (hereafter % a.s.) and close to 0 in response to some of the precipitation events.

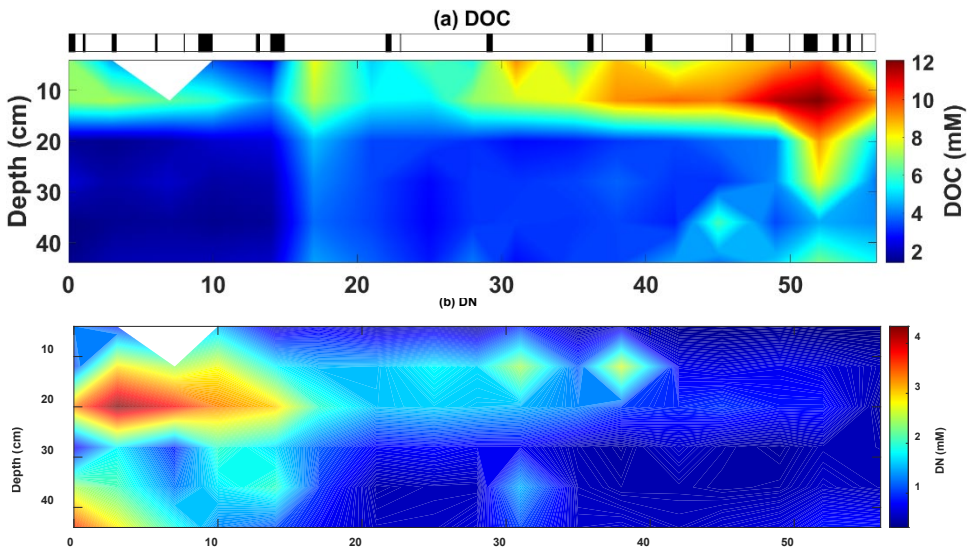

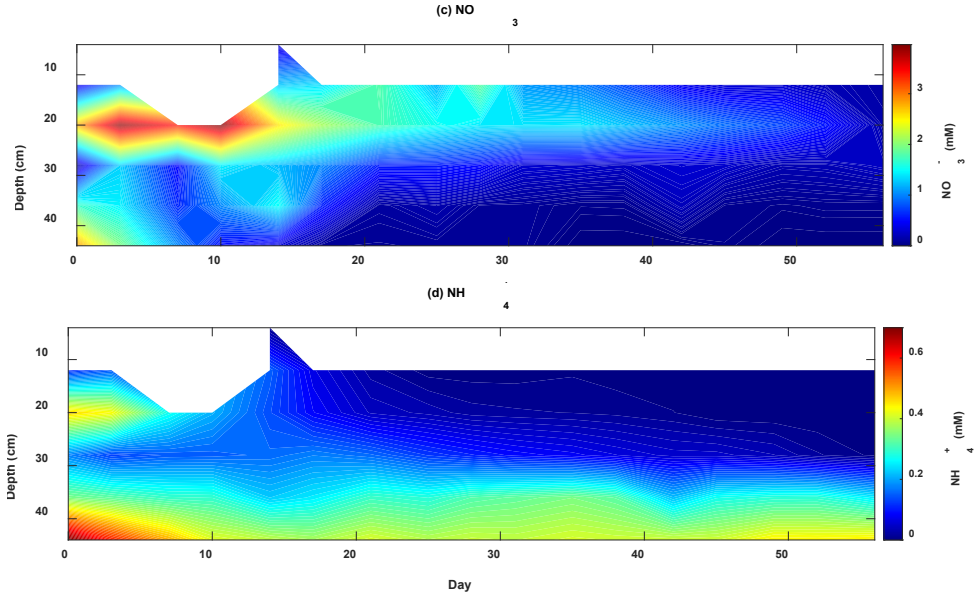

Figure 4: Chemical composition of porewater collected from lysimeter suction cups. The narrow bar plot at the top represents precipitation events and the widths of the bars correspond to the volume of rainwater delivered per precipitation event. (a) DOC concentration; (b) Dissolved nitrogen (DN) concentration; (c) Nitrate concentration; (d) Ammonium concentration. The white areas in the plot correspond to periods when the soil water content was too low to allow for the collection of water for all analyses.

Porewater was collected from 6 depths from day 0 to day 56 and analyzed for its chemical composition (**Figure 4,** see Fe(II), HS^-, SO_4^{2-} and Mn(II) concentration plots in **Figure S4**). DOC concentrations were highest in the top two layers of the lysimeter and increased with time following heavy precipitation events. Starting from day 50, a large increase in DOC concentration was observed below the 12-cm layer.

Nitrogen in porewater was measured in the form of total dissolved nitrogen (DN), NO_3^-, and NH_4^+. Collecting porewater samples from the layer 1 suction cup was difficult because of the low moisture content. As a result, nitrogen characterization was performed primarily on samples from layers 2-6 (**Figure 4b–4d**). At the beginning of the experiment, DN was abundant in layer 3 and layer 6, and NO_3^- mostly present in layer 3. NH_4^+ appeared primarily in layer 6, along with a lower concentration in layer 3. Within the first 10 days, NO_3^- was consumed deeper in the lysimeter (layer 6), while NH_4^+ was consumed at shallow depths (layer 3). After ~ 20 days, most of the NO_3^- in layer 3 was also consumed while NH_4^+ persisted until measurements stopped (day 56).

3.2 Microbial community analysis

The microbial community composition and total biomass concentration varied with depth (**Figure 5** and **Figure S1**).

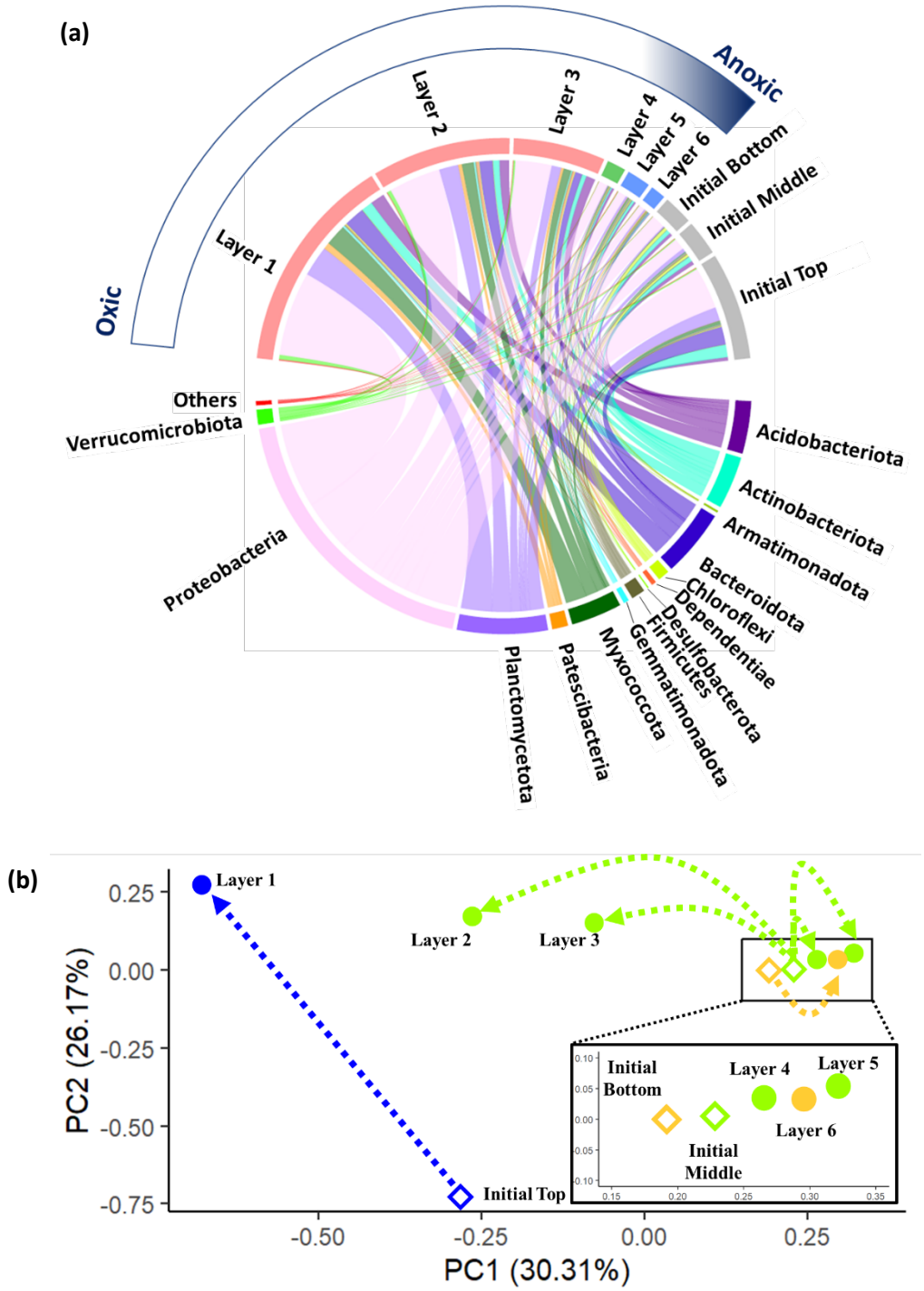

Figure 5: (a) The soil microbial composition at the phylum level as a function of depth in the beginning and the end of the experiment. The size of each block represents the absolute abundance. Phyla with a relative abundance less than 1% were assigned to 'others' in this figure. (b) Principal-component analysis of bacterial 16S rRNA gene composition and absolute abundance for microbial communities from various depths of the lysimeter at the beginning and the end of the experiment. Arrows were used to connect layers with their original microbial communities; different colors refer to different original communities.

Initially, the dominant phyla in the soil/leaf mixture (lysimeter top 10 cm) were *Proteobacteria* (43.08%), *Bacteroidota* (18.17%) and *Planctomycetota* (14.18%); in forest soil (lysimeter middle, 10-45 cm depth), the dominant phyla were *Proteobacteria* (36.71%), *Actinobacteriota* (15.90%) and *Planctomycetota* (11.93%); in coarse forest soil (bottom 5 cm), the dominant phyla were

Proteobacteria (52.33%), *Actinobacteriota* (16.03%) and *Chloroflexi* (11.81%). After 110 days of incubation, the dominant taxa varied across soil layers. In layers above the water table (layer 1, 2 and 3), the dominant phyla were *Proteobacteria* (43.35±1.12%), *Planctomycetota* (14.02±2.14%) and *Bacteroidota* (9.82±1.03%); in layers within the water table fluctuation zones (layer 4 and 5), the dominant phyla were *Proteobacteria* (47.45±9.14%), *Acidobacteriota* (10.37±3.78%) and *Actinobacteriota* (9.59±2.05); in layer below the water table (layer 6), the dominant phyla were *Proteobacteria* (45.19%), *Planctomycetota* (11.82%) and *Patescibacteria* (7.42%). Proteobacteria and Planctomycetota dominated in most soil samples we collected.

Principal-component analysis showed microbial community compositions from different depths at the end of the experiment compared to the original soil microbial community (**Figure 5b**). Along both PC1 (30.31% variance explained) and PC2 (26.17% variance explained), soil microbial communities in layers 4-6 retained microbial community compositions that are close to their original microbial communities, 'initial middle' and 'initial bottom'. On the other hand, although originating from the 'initial middle' community, layers 2&3 showed substantial change relative to the original microbial community and each other along PC1. Furthermore, the analysis suggested that layer 1 and its origin ('initial top') were distinct along both PC1 and PC2.

The 16S rRNA gene copy number (per gram of dry soil) was measured as a biomass marker for bacteria and archaea biomass cells in lysimeters. As soil samples were collected every 4 cm, spatial resolution of the microbial analysis is higher than that of the chemical analysis, so we do not refer to layers for part of the microbial analysis results. Results showed that bacterial biomass concentration decreased with depth from 0 to 25 cm and then remained at a relatively low level ($\leqslant 10^{10}$ 16S rRNA gene copies/gram dry soil) from 25 to 50 cm (**Figure S1a**). The highest bacterial biomass concentrations were found in the sample centered at 15.5 cm and spanning from 13 to 17 cm. Soil bacterial biomass concentrations increased with time, particularly in the top and middle samples (0-10 and 10-45 cm) and, conversely, decreased in the bottom samples (45-50cm). Mean values of bacterial biomass concentration increased by 79.41% in the top layer (0-10cm) and 72.93% in the middle layer (10-45 cm), and decreased by 51.18% in the bottom layer (45-50 cm). The distribution patterns of archaeal biomass concentrations were almost the same as bacteria, however, the concentrations of archaea were lower than that of bacteria by two orders of magnitude (**Figure S1b**) with the highest archaeal biomass concentration found at 11cm depth.

Data obtained from sequencing the DNA extracted from the soil microbiome were integrated into the 6 layers mentioned before and aggregated at each of the 5 radial positions. The local γ-diversity was computed for each position and layer, based on the aggregated results (**Figure S5**). We observed that the local γ-diversity decreased vertically with increasing depth for samples collected at the periphery of the lysimeter, while it remained relatively stable along depth at the center. Horizontally, local γ-diversity in the center site was much lower than periphery sites, particularly for layers 2&3.

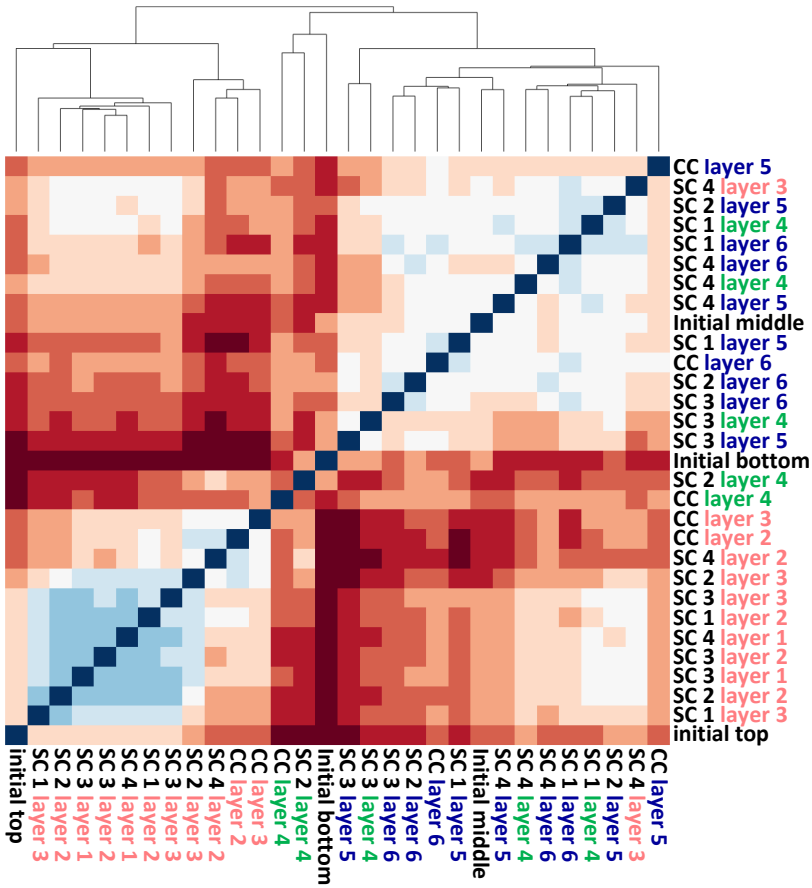

Figure 6: Clustergram of pairwise comparisons of soil microbial communities by using the Sorensen dissimilarity index. CC refers to 'Central Core' and SC refers to 'Side Core'. Blue color refers to similarity between two microbial communities and red color refers to dissimilarity between two microbial communities. Labels were color-coded according to their depth.

Pairwise comparison was conducted for soil microbial communities at various horizontal locations and depths and the original community by using the Sorensen dissimilarity index (**Figure 6**). Since this analysis only focused on the presence and absence of microbes, its result may vary from **Figure 5b**, which looked at both presence and abundance of microbes. As shown in the left bottom corner of **Figure 6**, layers 1-3 from most cores clustered together, suggesting similar microbial community compositions, which were also similar to the "initial top" microbial community. Layer 4 samples varied across cores with some different from all other samples, while others were similar to the community in layers 5&6 (from all cores). As shown in the right top corner of **Figure 6**, layers 5&6 from most cores clustered together, suggesting similar microbial community compositions. Moreover, the microbial community composition of layers 5&6 were also similar to the "initial middle" microbial community composition rather than the "initial bottom" composition, which contributed to half of initial layer 6 before the start of the experiment.

The Sorensen dissimilarity index was also calculated for the 6 layers of the lysimeter to compare differences in species distribution between locations in each layer (**Figure S6**). The spatial heterogeneity was relatively low for layers 1, 2 and 6, while the spatial heterogeneity was much higher for layers 3, 4 and 5. Especially for layer 4, the Sorensen dissimilarity index was higher than 0.4 for all sites, which suggest the microbial community composition is horizontally heterogenous within this layer.

The abundance of individual taxa was plotted as a function of depth and microorganisms that were identified in at least 4 individual samples were grouped into 10 groups according to the characteristics of their distribution pattern (**Figure S7**). Six of these patterns are shown in **Table 2** and the rest in **Table S1.** A few microorganisms were selected from some of the distribution patterns based on their metabolic potential (**Figure 7**) and the rest is shown in SI.

Pattern	Description
Pattern 1	Microbial concentration decreases with depth and below initial concentration
Pattern 2	Microbial concentration remains similar to the initial concentration along the entire depth
Pattern 3	Microbial concentration is stable above the initial concentration along the entire depth
Pattern 4	Microbial biomass is mainly found at the bottom and the concentration far exceeds the initial concentration
Pattern 5	Microbial biomass is mainly found at the top and the concentration far exceeds the initial concentration
Pattern 6	Microbial biomass is only found in the top 10 cm initially, concentration decreases with depth and drops below the initial concentration

Table 2: Description of different distribution patterns of microbes

Microbial metabolism was investigated and summarized for the 6 selected patterns, except for the large fraction of microorganisms for which no information is available (100 out of 302 taxa). Among the distribution patterns, we focused on those that exhibited clear dominance of aerobic or anaerobic taxa. In particular, patterns 1, 3, and 6 were characterized by taxa that include obligate aerobes representing more than 60% of overall taxa (27 out of 32, 13 out of 17 and 26 out of 30 taxa investigated, respectively). In contrast, pattern 4 was characterized by taxa that include obligate anaerobes representing more than 60% of overall taxa investigated (12 out of 18 taxa investigated). Pattern 2 showed a similar number of taxa that include obligate aerobe and anaerobes (18 and 13 out of 33 taxa investigated) while pattern 5 was characterized by high number of taxa that include obligate aerobes and facultative anaerobes (11 and 6 out of 16 taxa investigated).

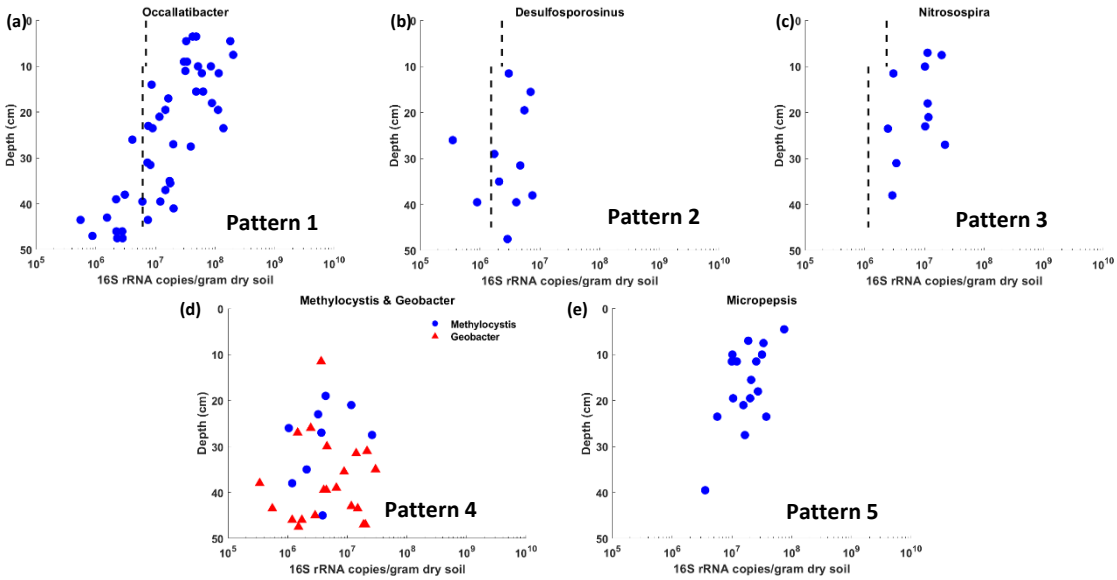

Figure 7: Distribution of microorganisms as a function of depth at the end of the experiment. Dashed lines represent the initial concentration before the experiment for each depth. The absence of a line signifies the concentration was below the detection limit. (a) *Occallatibacter;* (b) *Desulfosporosinus*; (c) *Nitrosospira*; (d) *Methylocystis & Geobacter;* (e) *Micropepsis*

Patterns 1, 2 and 6 included the most taxa amongst all patterns (45, 47 and 47, respectively). Patterns 1 and 6 represented taxa whose concentration decreases along depth, while pattern 2 corresponded to those taxa whose concentration remained similar to the initial concentration along the depth (i.e., no change). In contrast, patterns 4 and 5 included about 60% as many taxa as the patterns above (28 and 30, respectively).

First, we considered three genera harboring primarily strict aerobes. *Occallatibacter*, a genus encompassing strictly aerobic chemoorganotrophs, is distributed according to pattern 1, and was selected to represent microorganisms with aerobic metabolic potential (Foesel et al., 2016). The increase in *Occallatibacter* concentration from the initial to the final time point was mainly observed in the 0-30 cm range and its concentration decreased with depth.

Methylocystis is also a genus containing aerobes but distributing according to pattern 4. The bacteria are chemolithotrophic and able to grow on C1 compounds (Belova et al., 2013; Bowman et al., 1993; Dedysh et al., 2007). The initial concentration of *Methylocystis* was below the detection limit while at the end of the experiment, $10^6 – 10^7$ copies of 16S rRNA genes/g dry soil were found at 20-50 cm inside the lysimeter.

Nitrosospira is a genus that includes aerobic chemolithotroph, typically ammonium-oxidizing bacteria. It was selected from pattern 3 to represent nitrifiers (Head et al., 1993). The concentrations of *Nitrosospira* increased over the experimental period from 0 to 40 cm.

Next, we considered three genera harboring primarily strict anaerobes, *Geobacter*, *Desulfosporosinus,* and *Micropepsis.* Most *Geobacter* species are strictly anaerobic chemoorganotrophs, but a few were reported to be able to utilize O_2 as the sole electron acceptor (Lin et al., 2004; Lovley et al., 1993). *Geobacter* was also selected from pattern 4 and could represent microbes capable of iron and manganese respiration, as it reduces insoluble Fe(III) and Mn(IV) oxide to Fe(II) and Mn(II). The initial concentrations of *Geobacter* were too low for detection. However, at the end of the experiment, *Geobacter* was found mainly in the range of 25-50 cm at approximately 10^7 copies of 16S rRNA genes/g dry soil.

Desulfosporosinus is a genus of strict anaerobes and could represent sulfate-reducing bacteria due to its ability to reduce SO_4^{2-} to HS^- in the presence of organic carbon as the electron donor

(Robertson et al., 2001). It was selected from pattern 2. Initially, *Desulfosporosinus* was widely distributed within the soil in both the 0-10 cm and 10-45 cm zones. However, at the end of the experiment, this genus was only found from 10 to 50 cm depth with a near-constant concentration over depth. Comparing these values to the initial concentration suggests that the growth of *Desulfosporosinus* was limited.

Micropepsis species are strictly anaerobic and this genus was selected from pattern 5. It grows fermentatively on various organic carbon sources (Harbison et al., 2017). The initial concentration of *Micropepsis* was too low to be detectable. However, at the end of the experiment, *Micropepsis* was found at more than 10^7 copies of 16S rRNA genes/g dry soil mainly in the range of 0-30 cm.

3.3 Biogeochemical model simulations

The biogeochemical model developed by Miele et al. (2023) was used to simulate biogeochemical processes in the lysimeter. It was first used to reproduce E_h values as a function of time and depth. To evaluate the performance of the model, a comparison between measured and predicted E_h values is shown in **Figure S8**. In general, the model prediction matched the observed data quite well. However, E_h prediction errors were still found mainly at layers 5-6, where modeled E_h values reached close to zero during the experiment, which amplifies the errors calculated.

In addition, the biogeochemical model enables the prediction of the fraction of electrons transferred via the main biogeochemical processes as a function of time and depth (**Figure 8** and **S9**). The model suggests microbial activity in layers 1&2 was dominated by aerobic respiration and nitrification early in the experiment. However, the contribution of nitrification decreased sharply, and after day 10, only aerobic respiration remained (**Figure 8a** and **S9a**). For layer 3, nitrification and aerobic respiration also dominated early in the experiment and the contribution of nitrification decreased over time. However, unlike the layers above, the model indicates that nitrification continued to contribute > 10% to the overall electron transfer up until the end of the experiment (**Figure 8b**). In layer 4, where E_h values fluctuated in response to precipitation events, the dominant biogeochemical processes varied with the rise and fall of the water table. When water table rose, the dominant biogeochemical processes were mainly Fe(III) and Mn(IV) reduction, while when it fell, the dominant biogeochemical processes were mainly aerobic respiration, followed by oxidation of Fe(II), microbial Mn(II) oxidation, and nitrification (**Figure 8c**). Finally, in layers 5 & 6, the dominant biogeochemical process was Mn(IV) reduction from day 0 to day 35. After day 35, Fe(III) reduction was responsible for more than 50% of the electrons transferred, followed by Mn(IV) reduction and a small contribution of SO_4^{2-} reduction (**Figure 8d** and **S9b**).

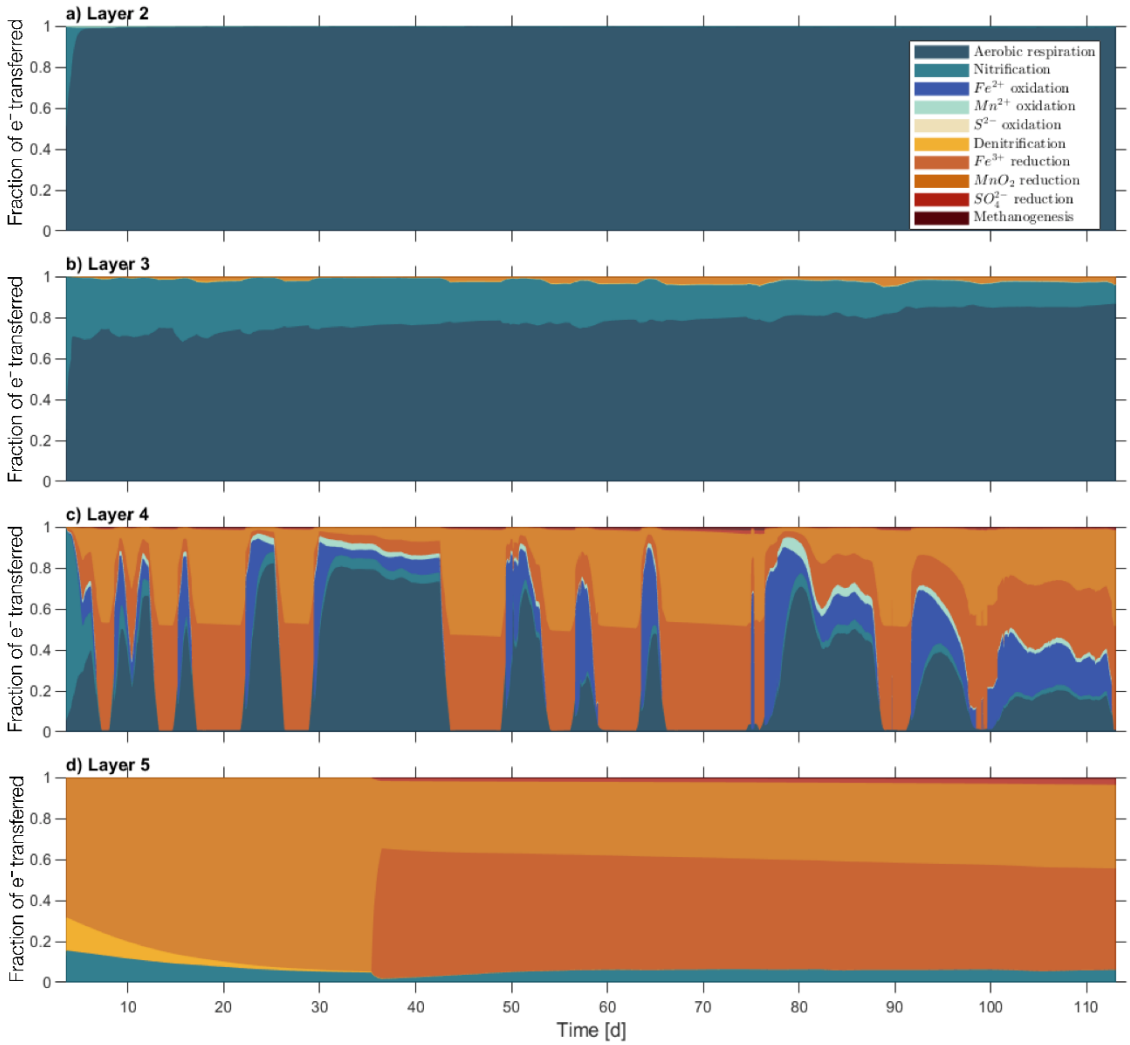

Figure 8: Fraction of electrons transferred as a result of specific biogeochemical processes as a function of depth and time. (a) layer 2; (b) layer 3; (c) layer 4; (d) layer 5

4. Discussion

4.1 The water table level controls biogeochemical processes

The physicochemical parameters measured by probes and electrodes, as well as the porewater chemical composition were integrated to develop an understanding of the relevant biogeochemical processes within the lysimeter, which were linked to an important parameter – water table elevation (**Table S2**), a byproduct of soil moisture dynamics. As shown in **Figure 3c**, the water table fluctuated owing to the imposed rainfall from 25-40 cm. The response of soil moisture content to precipitation was muted in layers 1 and 3 compared to layer 5 (there were no sensors in layers 2 and 4). This suggests the transport of water past layers 1 and 3 and its accumulation at layer 5. Three sharp increases of soil moisture content in layer 3 after heavy precipitation events are interpreted as transient water table increases (**Figure 3c**).

Based on the range of E_h values, the lysimeter can be divided into three zones: an oxidized zone that remained above the water table throughout the experiment (layers 1-3, 0-24 cm); a fluctuating zone where the water table oscillated and the soil redox conditions fluctuated between oxidized and reduced conditions (layer 4, 24-32 cm); and a strongly reduced zone that remained at the lower boundary or below the water table throughout the experiment (layers 5&6, 32-50 cm). As the transport of O_2 is strongly affected by soil humidity and the concentration of DOis affected by precipitation events (**Figure 4a**), it is not surprising that DO concentrations were strongly

correlated to water table levels **(Table S2)**. This also resulted in a strong correlation between E_h and water table elevations.

Here, we integrate the geochemical data to probe differences between the three zones.

Oxic zone: In this zone (layers 1-3), O_2 diffusion into the soil resulted in DO concentrations close to equilibrium with the atmosphere for most of the experiment. However, they showed short-term dips after most precipitation events, which may be caused either by enhanced microbial respiration due to the replenishment of water in a previously dry soil, by O_2 transport being hindered by a temporary increase in soil moisture content, or both. In terms of DOC, although the artificial rainwater applied contains no organic carbon, the DOC concentration increases after precipitation events (e.g., in layers 1&2 starting from day 30). This correlation can be explained by the release of DOC from the soil-leaf mixture into porewater through leaf litter decomposition by both fungi and bacteria (Lladó et al., 2017). This could occur as the result of enhanced microbial processes in response to either an increase in moisture content and/or leaching of DOC from particulate organic carbon. Within this zone, E_h values remained at 600 to 800 mV during the entire experiment, which indicates that in the three top layers, aerobic respiration is dominant throughout the experiment. E_h values in layer 3 were slightly higher than E_h values layers 1&2, which we attribute to higher TOC content in those layers due to the high leaf content. Indeed, high TOC content may increase the rate of O_2 consumption and result in lower DO and E_h (Husson, 2013). Considering the NH_4^+ and NO_3^- concentration changes in layer 3, both nitrification and denitrification might exist in this layer at the beginning of the experiment, however, with the consumption of NH_4^+ and NO_3^-, the magnitude of nitrification and denitrification activity significantly decreased, which was also confirmed with the decreasing N_2O flux from the soil surface (**Figure S10a**). The geochemical data in layer 3 suggests an overestimation of nitrification by the biogeochemical model due to its lower TOC content (**Figure 8b**). Except for this, the interpretation based on the observed physicochemical data is consistent with the biogeochemical model prediction that the dominant biogeochemical process in these layers is aerobic respiration, with nitrification occurring as well (**Figures 8a-8b, S9a**). However, this interpretation is not fully consistent with field observations, in which anaerobic processes co-exist with aerobic respiration even though it is the dominant biogeochemical process (Hall et al., 2013). Such variation may be attributed to multiple factors. On one hand, the interpretation was mainly based on the E_h values measured by redox electrodes, which only reflect the redox conditions of bulk soil and do not capture the E_h of anaerobic microsites (Dorau et al., 2022). On the other hand, a few of the limited number of porewater samples that could be collected from the unsaturated zone showed trace amount of Fe(II), Mn(II) and HS^-, supporting the presence of anaerobic microbial processes in the oxidized zone.

Redox-fluctuating zone (layer 4): In the fluctuating redox zone, the DO concentration changed according to the water table level. It increased when the water table fell and decreased when the water table rose. The water table reached its lowest levels late in the experiment (day 60-110) (**Figure 3c**), while the DO concentrations in layer 4 did not increase to the same extent as it did early (day 0-60) in the experiment (i.e., up to 60% a.s.) despite the low water table level. This occurrence is interpreted as a higher O_2 consumption rate within the fluctuating zone. Indeed, although the DOC concentration was low at this depth early in the experiment, precipitation-induced DOC release and transport led to an increase in DOC in this and deeper layers. Evidence of DOC downward transport can be observed shortly after day 50 with a sharp increase in DOC concentrations at all depths. This resulted in a large dip in the E_h values in layers 4-6. Indeed, the increased availability of DOC fueled the depletion of an electron acceptor and the shift to another, as indicated by E_h values at these layers (**Figure 3a**) and the biogeochemical model results (**Figure 8c**).

In layer 4, E_h values fluctuated with precipitation events from day 0 to day 60 but remained oxidizing, suggesting that aerobic respiration or perhaps denitrification could take place along with

the oxidation of Fe(II) and Mn(II). The decrease in E_h values following precipitation events may be attributed to decreasing DO as a result of a rising water table and a shift in the electron acceptor, in this case, to Mn(IV). This inference is supported by experimental data, an increase in Mn(II) concentrations, as well as by the model, that predicts Mn(IV) and Fe(III) reduction as the main processes when E_h and DO decrease (**Figure 8c**). After day 60, although E_h values still fluctuate with precipitation events, the range of values becomes more negative. Combined with the large concentration of DOC transported from top layers downward starting at day 50, we propose that higher DOC concentrations enhanced the DO consumption rate, thus, when the water table rises or falls, the environment can quickly switch from oxidizing to reducing. This interpretation of dominant biogeochemical processes is consistent with the important role of coupled Fe/Mn-C cycling in forest soil redox fluctuating zone that have been reported in previous literature (Hall & Silver, 2013; Jones et al., 2018; Li et al., 2021; Silver et al., 2013).

Anoxic zone: In the anoxic zone and the fluctuating zone region closest to the anoxic zone (layers 5&6), the DO concentration remained close to zero throughout the experiment. In layers 5&6, from day 0 to day 50, E_h values gradually decrease and, based on E_h values and Mn(II) concentrations, the major metabolism is presumed to be Mn(IV) reduction. Based on the change in NO_3^- concentration (**Figure 4c)**, denitrification may occur from day 0 to day 10. After day 50, a sharp decrease of E_h values were observed in layers 5&6, which happened simultaneously with significant amount of DOC being transported downward and Fe(II) starting to appear in these layers. Thus, it is possible that the DOC transported enhanced the consumption of e^- acceptors and drove Fe(III) reduction in these two layers, thus the dominant biogeochemical processes in these two layers were Fe(III) and Mn(IV) reduction. This interpretation is supported by the model that identifies Mn(IV) and Fe(III) reduction as the dominant metabolisms (**Figures 8d** and **S9b**). Previous literature also reported Fe(III) reduction as the main contributor to anaerobic carbon oxidation in forest soil that received a large amount of precipitation (Dubinsky et al., 2010), which further supports our interpretation. Surprisingly, intermittent increases in E_h values were observed in layer 5 during this period. Considering that they occurred shortly after precipitation events, they could be explained by the transport of more oxidizing, O_2-containing, porewater to layer 5 from above.

4.2 Microbial community diversity and abundance

The distribution of the microbial community within the lysimeter was investigated as a function of depth and radial position. As shown in **Figure S1a**, biomass concentration decreased with depth but showed no significant change with radial position (**Table S3**). DO concentrations and DOC availability decrease with depth and likely play key roles in controlling biomass concentration via aerobic respiration. In other words, the most biomass buildup was driven by aerobic respiration activity which was boosted by high DOC and DO, which is expected from the energy yield of this metabolism (Saltveit, 2019).

β-diversity that describes the similarity/dissimilarity amongst microbial communities was calculated by the pairwise Sorensen dissimilarity index (**Figure 6**). It suggested a clear stratification of microbial communities along depth, according to three groups: 1) layers 1-3, 2) layer 4 and 3) layers 5&6. This stratification was identical to that evidenced by the lysimeter hydrological regimes supporting the impact of hydrological conditions on the soil microbial community.

Oxic zones: Layer 1 originated from the "initial top" community while layers 2 and 3 originated from the "initial middle" community. At the end of the experiment, all three layers were more similar to "initial top" community, rather than "initial middle" community (**Figure 6**), which suggests microbial community composition changes in layers 2 and 3 potentially via transport and growth. These changes were more evident in **Figure 5b**, where layers 2&3 communities show large differences when compared to their original composition, suggesting input of microorganisms (for example *Dongia*, *Leptothrix*) from the layer above.

Anoxic zones: Layer 5 originated from "initial middle" and layer 6 originated equally from both "initial middle" and "initial bottom" communities. At the end of the experiment, layers 5 and 6 were similar to one another and to the "initial middle" community. The "initial bottom" community only differs from the "initial middle" community as a result of the retention of only the coarse particle fraction (> 50µm). Thus, its species richness was negatively impact by the sieving process (**Figure S5**). However, as layer 6 is a mixture of the two initial communities, its initial composition included the "initial middle" taxa. The fact that both layers are similar to "initial middle" community suggested limited growth may happen within anoxic zones. This was evidenced by the close positions of layers 5&6 and "initial middle" community in the principal-component analysis (**Figure 5b**).

Redox-fluctuating zones: Layer 4 originated from the "initial middle" community but its microbial community composition at the end of the experiment varied amongst cores. For some cores, the layer 4 communities were similar to the "initial middle" community as well as to the communities in anoxic zones, suggesting limited change in the biomass and diversity of the microbiome within these cores. In contrast, others were not similar to "initial middle" or any other community, suggesting a unique community adapted to the fluctuating redox conditions. The heterogeneity of layer 4 samples will be discussed later in this section.

Next, we probed whether a constant redox state may result in greater microbial diversity and distinct radial distribution of the microbial community as compared to a fluctuating redox state. Based on the literature (Degens et al., 2001; Fierer et al., 2003; Peralta et al., 2014; Rühle et al., 2015), we expected the greatest microbial diversity at the redox transition zone, near the middle of the lysimeter. Instead, we observed that the local γ-diversity of soil samples in the lysimeter periphery showed a decreasing trend as a function of depth, suggesting that the overall species richness decreased with depth (**Figure S5**). This trend may be attributed to the decreasing DOC concentration as a function of depth. High organic carbon content in the top layers promotes the growth of microorganisms, while in deeper layers, competition for organic carbon limits growth (Fontaine et al., 2003). In other words, organic carbon availability overprints other processes that may increase the microbial diversity in redox fluctuating zones and results in a clear downward trend of species richness with depth. Lladó et al. (2017) also reported the important role of the vertical gradient of bioavailable organic carbon in characterizing the forest soil bacteria community. Therefore, capturing the spatial complexity of a soil environment allows the identification of dominant effects that would not otherwise be delineated in batch systems receiving the same amount of DOC. Moreover, despite the nominally oxic environment in the top layers, the presence of low-permeability microsites also provided anoxic microenvironments for anaerobes (Silver et al., 1999), furthering species richness. This is evidenced by the growth of obligate anaerobes in top layers (**Figure 7e**).

Analyzing the microbial distribution patterns along the radial direction we found that, in contrast to samples in the SC positions, soil samples in the CC position exhibited low local γ-diversity along the entire depth, suggesting that overall species richness is low at all depths in the central position. This occurrence may be due to preferential flow paths along the lysimeter wall, providing more DOC and thus more opportunity for a diverse community to grow at the SC rather than CC locations (Franklin et al., 2021).

In addition to the pairwise Sorensen dissimilarity index analysis (**Figure 6**), β-diversity was also calculated using the Sorensen dissimilarity index for the comparison of multiple samples as a function of their horizontal position, and the Pearson correlation coefficient for vertical dissimilarity (**Figure S6 & S11**). The Pearson correlation coefficient revealed that the similarity between microbial communities decreased with their vertical distance (**Figure S11**). More specifically, considering the vertical distance between any two locations, the greater the distance, the lower the similarity across microbial communities. This suggests that vertical distance plays an

important role in controlling the microbial community composition, supporting the role of microbial transport in inoculating lower layers.

The Sorensen dissimilarity index showed high radial spatial heterogeneity within layers in and around the redox fluctuating zone (**Figure S6**), which was supported by the heterogeneous β-diversities of layer 4 sample in **Figure 6**. This is likely due to the vertical heterogeneity of the water table level. We propose that the water table rise estimated based on readings from the tensiometer at 36 cm depth represents the bulk water table level while capillary fringe effects actually result in variable water saturated zones through the lysimeter's horizontal cross-section (Ronen et al., 2000). This effect would not significantly affect soil that remains permanently above or below the water table (**Figure S6**), as it retains a relatively constant moisture content. However, for soils within or close to the redox fluctuating zone, individual locations within a single soil layer would be exposed to distinct hydrological conditions, and thus a distinct influx of DOC, DO and other nutrients, explaining the radial spatial heterogeneity of microbial communities and the discrepancy between the model with the data at those depths.

The temporal change observed in the microbial community, from its uniform initial composition to its final stratified composition, was investigated spatially, as a function of hydrological regime (and associated static or fluctuating redox potential). Layers 2-5 originated from the same soil microbial community ('initial middle') and were incubated under three different hydrological regimes (oxic, fluctuating, and anoxic). The principal-component analysis (**Figure 5b**) shows that there is little change observed in the microbial community in the bottom layer (layer 5, permanently anoxic), whereas the community in the top layers (layers 2&3, permanently oxic) have changed considerably over the 110 days of the experiment. In addition, the two oxic layers, while originating from the same initial microbial community differed from one another, which may be attributed to the difference in their DOC concentrations (**Figure 4a),** and to the impact of the "initial top" community (**Figure 5b**). In the middle layer (layer 4, fluctuating between oxic and anoxic), microbial community compositions showed little change compared to their initial microbial community (**Figure 5b**). Though **Figure 6** suggested some layer 4 samples were quite different from the "initial middle" community, this difference was explainable by methodological differences. In **Figure 6,** the β-diversity analysis only considered the existence of microbes, which may overestimate the dissimilarity due to the presence of microbes at low concentrations. On the other hand, the principal-component analysis considered both the existence and the abundance of microbes, producing a more complete view of the change in the community.

In general, according to **Figure S7** the number of taxa containing obligate aerobes dominated at the end of the experiment (representing 140 out of 202 taxa investigated) and they were mainly found distributed according to patterns 1 and 6. Both patterns were characterized by microbial concentrations decreasing with depth, which was consistent with the DO gradient along the depth inside the lysimeter. The number of taxa including obligate anaerobes were found to be the second largest overall inside the lysimeter (40 out of 202 taxa investigated). They were found to be mainly distributed according to patterns 2 and 4. As pattern 2 evidences no change in abundance relative to the initial time, limited growth would be expected for those anaerobes that follow that pattern of distribution. On the other hand, significant growth of microbes was observed in pattern 4. Thus, growth of most taxa containing obligate anaerobes mainly happened in 25-50 cm depth, which consists of the redox fluctuating and anoxic zones.

4.3 Comparison between biogeochemical model and community analysis

To evaluate the accuracy of the biogeochemical model developed by Miele et al. (2023) and better predict the biogeochemical processes within the soil, the dominant biogeochemical processes predicted by the model were compared with the metabolic potential of the community indicated by the biomass concentration and the measured growth of microbes harboring the metabolic potentials of interest.

Aerobic respiration was predicted to be the dominant biogeochemical process in the oxic layers (layer 1-3) and also in the fluctuating zone (layer 4) when the water table falls (**Figure 8a-c, Figure S9a**). Amongst bacteria identified in the soil, *Occallatibacter* was chosen to represent aerobic respiration (**Figure 7a**). Taxa containing obligate aerobes were mainly distributed according to patterns 1 and 6 and most of them were mainly detected from 0 to around 30 cm depth and their concentration decreased over depth, which was consistent with the gradient of DOC and DO concentrations. Compared to their initial concentrations (or, if not detectable, the initial concentrations in the layer above), the concentrations of obligate aerobes were also found to have increased from the soil surface to around 0-30 cm due to growth and potential transport of microbes. Their distribution confirmed the prediction from the model that aerobic respiration was the dominant biogeochemical processes in these layers.

Based on the biogeochemical model, nitrification largely contributed to electron transfer in layers 1-4 at the beginning of the experiment, however, after around 10-15 days, the contribution of nitrification decreased to close to 0 in layers 1&2. During the rest of the experiment, nitrification continued to contribute to electron transfer in layers 3&4 when the water table fell. *Nitrosospira* was selected to represent microbes with nitrification potential (**Figure 7c**). It was mainly detected from 10 to around 30 cm deep, and although its concentration as a function of depth did not fit any pattern, growth of *Nitrosospira* was detected based on an increase relative to its initial concentration. At the end of the experiment, nitrification was still predicted to be significant in layer 3 by the model, while limited nitrification was predicted to be found in other layers. However, the concentration of *Nitrosospira* within this layer showed no difference with other layers in which *Nitrosospira* was detected. Potential reasons to explain this difference between observation and model prediction might be 1) detected 16S rRNA genes may not only represent live cells, dead cells could also contribute to the signal; or 2) the contribution of nitrification to electron transfer in this layer is overestimated by the model, which might be an mis-interpretation of the slightly higher E_h values caused by lower DOC concentrations in layer 3 compared to layers 1&2.

Fe(III) reduction and Mn(IV) reduction were predicted to be the dominant biogeochemical processes in layers 5&6 and also in layer 4 when the water table rises. The genus *Geobacter* was chosen to represent bacteria capable of Fe(III) and Mn(IV) reduction. As shown in **Figure 7d**, *Geobacter* was mainly found in soil from 25 to 50 cm deep and exhibited significant growth (from non-detectable to 10^7 gene copies/g dry soil). This finding was consistent with the biogeochemical model prediction of metal reduction and the detection of Fe(II) and Mn(II) at these depths (**Figure S4a&4b**).

SO_4^{2-} reduction was predicted to have limited contribution to electron transfer in layers 5&6 and also layer 4 when the water table rises. The genus *Desulfosporosinus* was selected to represent sulfate-reducing bacteria. As shown in **Figure 7b**, *Desulfosporosinus* was detected from 10 to 50 cm deep and some growth of *Desulfosporosinus* was observed in layers from 30 to 50 cm, which was consistent with the model prediction. However, some *Desulfosporosinus* growth was also found in the 10 to 20 cm layer, which was not predicted by the model. Potential reasons to explain this could be some SO_4^{2-} reduction occurred in low-permeability microsites, which is supported by the increase of HS^- in this layer starting day 50 (**Figure S4d**).

Besides biogeochemical processes predicted by the model, there may be other metabolisms taking place in the lysimeter as suggested by the metabolic potential of other bacteria identified in the soil. The methylotroph *Methylocystis* was detected from 20 to 50 cm, while it was not detectable in the initial samples (**Figure 7d**). Because it only utilizes C1 compounds, its growth suggests that methylotrophy or methanotrophy took place in those layers. The amplicon sequencing primers we selected were predicted to poorly amplify Archaea, therefore it is not surprising that no methanogens were detected despite detecting the production of CH_4 in the latter part of the experiment (**Figure S10b**).

Moreover, although fermentation was not included in the model, unsurprisingly, fermenters were detected in the soil. Most taxa containing fermenters were distributed according to patterns 2 and 4 (10 and 8 taxa, respectively). This suggested the growth of most fermenters in redox fluctuating zones and anoxic zones. However, fermenters distributing according to pattern 4, such as *Micropepsis*, were present in the soil in the 0 to 30 cm layer at concentrations of $3.6 \times 10^6 \sim 7.5 \times 10^7 16S\ rRNA\ gene\ copies/g\ dry\ soil$ while it was undetectable in the initial soil (**Figure 7e**). Though E_h values within these layers indicated oxidizing conditions throughout the experiment, especially for layers 1-3, fermentation may still occur in low-permeability and DOC-rich microsites. Spatial heterogeneity expressed by oxic or anoxic niches in unexpected regions are difficult to capture at this spatial resolution on both the experimental and modelling sides (Dorau et al., 2023). Thus, further improvement would be needed to better account for the potential effects of microsites on biogeochemical processes and microbial growth in soil.

The combination of community analysis with the biogeochemical model validates model outputs, as the distribution and growth and microbes with metabolic potential involved in the model were consistent with predictions made by the model. However, the community analysis also revealed that the biogeochemical may need further improvement by 1) involving more biogeochemical processes, such as methanotrophy and fermentation, for more comprehensive predictions; 2) considering the effects of microsites on biogeochemical processes and microbial growth, especially in DOC-rich top layers. An additional limitation in the experimental design is that despite substantial efforts to uniformly pack the soil, preferential flow paths still formed and impacted the homogeneity of the system.

5. Conclusions

An elaborate lysimeter-scale experiment was conducted to simulate natural forest soil receiving realistic precipitation and including leaf litter as a source of C and N. The daily precipitation was modulated to generate a Marked Poisson process whose mean is compatible with Switzerland's yearly mean value (and thus in the conditions where the soil forest has evolved). Contrary to soil within a redox-stable environment (i.e., permanently oxic or anoxic), the soil microbial community within redox-fluctuating zones showed a horizontally heterogeneous composition, which could be explained by the variable water saturation in distinct zones within a horizontal cross section, most resulting from capillary fringe effects or unavoidable preferential infiltration pathways.

Depth-resolved geochemical data and microbial analysis provided insight into the contradictory findings reported in the literature regarding microbial community diversity within redox fluctuating zones that could not have been extracted from more typical batch experiments. Previous work has either reported increased diversity as a result of redox fluctuation or no change in diversity relative to redox-static conditions. We propose that the depth-resolved analysis used here enables the capture of all the parameters that potentially contribute to the compositional trajectory of a microbial community. In particular, this work clearly evidenced the impact of the DOC gradient along depth as a major determinant of microbial community composition that overprinted the impact of redox fluctuation on the microbiome. Thus, taken on their own, redox fluctuations may indeed result in greater microbial diversity but these fluctuations rarely occur in isolation. Unsurprisingly, a comprehensive approach involving soil lysimeters and modeling provides a more complete understanding of the drivers of microbial community variations in soil.

Remarkably, the predicted metabolisms via the biogeochemical model developed by Miele et al. (2023) matches the distribution and growth of microbes with corresponding metabolic potential in most cases. Thus, here, we were able to recognize the dominant biogeochemical processes under different redox conditions: aerobic respiration under oxic condition; coupled Fe/Mn-C cycling under redox fluctuating condition and Fe/Mn reduction under anoxic condition. However, as revealed by the microbial analysis, due to current model limitations, we are unable to evaluate

the importance of certain relevant biogeochemical processes and underestimated the potential effect of anoxic microsites in DOC-rich oxic layers.

Acknowledgement

The authors acknowledge key funding provided by the Swiss National Science Foundation through its Grant CRSII5_186422. Many thanks to Colin Volet, Jantina van der Meer and Natalia Andrea Montoya Arévalo for providing help in the experiment process, Samir Simon Suweis for providing valuable suggestions in microbial analysis, Matti Barthel and Johan Six for N_2O site-preference analysis and Jana von Freyberg for providing the rainfall composition data. Lastly, we would like to extend our sincere thanks to the Central Environmental Laboratory and Mass Spectrometry – Elemental Analysis platform at EPFL and the Lausanne Genomic Technologies Facility in University of Lausanne for help with sample analysis.

Data Availability

The sequencing data for all samples were uploaded to GenBank databased (project number: PRJNA1098031)

References:

Ambus, P., Zechmeister-Boltenstern, S., & Butterbach-Bahl, K. (2006). Sources of nitrous oxide emitted from European forest soils. In *Biogeosciences* (Vol. 3). www.biogeosciences.net/3/135/2006/

Andermann, T., Antonelli, A., Barrett, R. L., & Silvestro, D. (2022). Estimating Alpha, Beta, and Gamma Diversity Through Deep Learning. *Frontiers in Plant Science*, *13*. https://doi.org/10.3389/fpls.2022.839407

Baselga, A. (2010). Partitioning the turnover and nestedness components of beta diversity. *Global Ecology and Biogeography*, *19*(1), 134–143. https://doi.org/10.1111/j.1466-8238.2009.00490.x

Batjes, N. H. (1996). Total carbon and nitrogen in the soils of the world. *European Journal of Soil Science*, *47*(2), 151–163. https://doi.org/10.1111/j.1365-2389.1996.tb01386.x

Belova, S. E., Kulichevskaya, I. S., Bodelier, P. L. E., & Dedysh, S. N. (2013). Methylocystis bryophila sp. nov., a facultatively methanotrophic bacterium from acidic Sphagnum peat, and emended description of the genus Methylocystis (ex Whittenbury et al. 1970) Bowman et al. 1993. *International Journal of Systematic and Evolutionary Microbiology*, *63*(Pt_3), 1096–1104. https://doi.org/10.1099/ijs.0.043505-0

Berardi, D., Brzostek, E., Blanc-Betes, E., Davison, B., DeLucia, E. H., Hartman, M. D., Kent, J., Parton, W. J., Saha, D., & Hudiburg, T. W. (2020). 21st-century biogeochemical modeling: Challenges for Century-based models and where do we go from here? *GCB Bioenergy*, *12*(10), 774–788. https://doi.org/10.1111/gcbb.12730

Bonan, G. (2019). *Climate Change and Terrestrial Ecosystem Modeling*. Cambridge University Press. https://doi.org/10.1017/9781107339217

Bowman, J. P., Sly, L. I., Nichols, P. D., & Hayward, A. C. (1993). Revised Taxonomy of the Methanotrophs: Description of Methylobacter gen. nov., Emendation of Methylococcus, Validation of Methylosinus and Methylocystis Species, and a Proposal that the Family Methylococcaceae Includes Only the Group I Methanotrophs. *International Journal of Systematic Bacteriology*, *43*(4), 735–753. https://doi.org/10.1099/00207713-43-4-735

Bremner, J. M. (1997). Sources of nitrous oxide in soils. In *Nutrient Cycling in Agroecosystems* (Vol. 49). Kluwer Academic Publishers.

Calabrese, S., & Porporato, A. (2019). Impact of ecohydrological fluctuations on iron-redox cycling. *Soil Biology and Biochemistry*, *133*, 188–195. https://doi.org/10.1016/j.soilbio.2019.03.013

Conrad, R. (2009). The global methane cycle: recent advances in understanding the microbial processes involved. *Environmental Microbiology Reports*, *1*(5). https://doi.org/10.1111/j.1758-2229.2009.00038.x

DeAngelis, K. M., Silver, W. L., Thompson, A. W., & Firestone, M. K. (2010). Microbial communities acclimate to recurring changes in soil redox potential status. *Environmental Microbiology*, *12*(12), 3137–3149. https://doi.org/10.1111/j.1462-2920.2010.02286.x

Degens, B. P., Schipper, L. A., Sparling, G. P., & Duncan, L. C. (2001). Is the microbial community in a soil with reduced catabolic diversity less resistant to stress or disturbance? *Soil Biology and Biochemistry*, *33*(9), 1143–1153. https://doi.org/10.1016/S0038-0717(01)00018-9

Dorau, K., Uteau, D., Hövels, M. P., Peth, S., & Mansfeldt, T. (2022). Soil aeration and redox potential as function of pore connectivity unravelled by <scp>X-ray</scp> microtomography imaging. *European Journal of Soil Science*, *73*(1). https://doi.org/10.1111/ejss.13165

Dorau, K., Uteau, D., Maisch, M., Kappler, A., Peth, S., & Mansfeldt, T. (2023). Redoxtrons – An experimental system to study redox processes within the capillary fringe. *European Journal of Soil Science*, *74*(1). https://doi.org/10.1111/ejss.13347

Drenovsky, R. E., Vo, D., Graham, K. J., & Scow, K. M. (2004). Soil Water Content and Organic Carbon Availability Are Major Determinants of Soil Microbial Community Composition. *Microbial Ecology*, *48*(3), 424–430. https://doi.org/10.1007/s00248-003-1063-2

Dubinsky, E. A., Silver, W. L., & Firestone, M. K. (2010). Tropical forest soil microbial communities couple iron and carbon biogeochemistry. *Ecology*, *91*(9), 2604–2612. https://doi.org/10.1890/09-1365.1

Federal Office of Meteorology and Climatology MeteoSwiss. (2021, December 17). *Normal values per measured parameter*. https://www.meteoswiss.admin.ch/services-and-publications/applications/ext/climate-normtables.html

Fierer, N., Schimel, J. P., & Holden, P. A. (2003). Influence of Drying-Rewetting Frequency on Soil Bacterial Community Structure. *Microbial Ecology*, *45*(1), 63–71. https://doi.org/10.1007/s00248-002-1007-2

Foesel, B. U., Mayer, S., Luckner, M., Wanner, G., Rohde, M., & Overmann, J. (2016). Occallatibacter riparius gen. nov., sp. nov. and Occallatibacter savannae sp. nov., acidobacteria isolated from Namibian soils, and emended description of the family Acidobacteriaceae. *International Journal of Systematic and Evolutionary Microbiology*, *66*(1), 219–229. https://doi.org/10.1099/ijsem.0.000700

Fontaine, S., Mariotti, A., & Abbadie, L. (2003). The priming effect of organic matter: a question of microbial competition? *Soil Biology and Biochemistry*, *35*(6), 837–843. https://doi.org/10.1016/S0038-0717(03)00123-8

Franklin, S. M., Kravchenko, A. N., Vargas, R., Vasilas, B., Fuhrmann, J. J., & Jin, Y. (2021). The unexplored role of preferential flow in soil carbon dynamics. *Soil Biology and Biochemistry*, *161*, 108398. https://doi.org/10.1016/j.soilbio.2021.108398

Gordon, H., Haygarth, P. M., & Bardgett, R. D. (2008). Drying and rewetting effects on soil microbial community composition and nutrient leaching. *Soil Biology and Biochemistry*, *40*(2), 302–311. https://doi.org/10.1016/j.soilbio.2007.08.008

Grunwald, D., Fender, A.-C., Erasmi, S., & Jungkunst, H. F. (2012). Towards improved bottom-up inventories of methane from the European land surface. *Atmospheric Environment*, *51*. https://doi.org/10.1016/j.atmosenv.2012.01.025

Haberer, C. M., Rolle, M., Cirpka, O. A., & Grathwohl, P. (2012). Oxygen Transfer in a Fluctuating Capillary Fringe. *Vadose Zone Journal*, *11*(3), vzj2011.0056. https://doi.org/10.2136/vzj2011.0056

Hall, S. J., McDowell, W. H., & Silver, W. L. (2013). When Wet Gets Wetter: Decoupling of Moisture, Redox Biogeochemistry, and Greenhouse Gas Fluxes in a Humid Tropical Forest Soil. *Ecosystems*, *16*(4), 576–589. https://doi.org/10.1007/s10021-012-9631-2

Hall, S. J., & Silver, W. L. (2013). Iron oxidation stimulates organic matter decomposition in humid tropical forest soils. *Global Change Biology*, *19*(9), 2804–2813. https://doi.org/10.1111/gcb.12229

Harbison, A. B., Price, L. E., Flythe, M. D., & Bräuer, S. L. (2017). Micropepsis pineolensis gen. nov., sp. nov., a mildly acidophilic alphaproteobacterium isolated from a poor fen, and proposal of Micropepsaceae fam. nov. within Micropepsales ord. nov. *International Journal of Systematic and Evolutionary Microbiology*, *67*(4), 839–844. https://doi.org/10.1099/ijsem.0.001681

Head, I. M., Hiorns, W. D., Embley, T. M., McCarthy, A. J., & Saunders, J. R. (1993). The phylogeny of autotrophic ammonia-oxidizing bacteria as determined by analysis of 16S ribosomal RNA gene sequences. *Journal of General Microbiology*, *139*(6), 1147–1153. https://doi.org/10.1099/00221287-139-6-1147

Hirano, S., Matsumoto, N., Morita, M., Sasaki, K., & Ohmura, N. (2013). Electrochemical control of redox potential affects methanogenesis of the hydrogenotrophic methanogen *Methanothermobacter thermautotrophicus*. *Letters in Applied Microbiology*, *56*(5), 315–321. https://doi.org/10.1111/lam.12059

Huang, P. M., Yuncong Li, & Malcolm E. Sumner. (2011). *Handbook of soil sciences: properties and processes*. CRC press.

Hungate, B. A., & Koch, G. W. (2003). GLOBAL CHANGE | Biospheric Impacts and Feedbacks. In *Encyclopedia of Atmospheric Sciences* (pp. 876–886). Elsevier. https://doi.org/10.1016/b0-12-227090-8/00472-3

Husson, O. (2013). Redox potential (Eh) and pH as drivers of soil/plant/microorganism systems: a transdisciplinary overview pointing to integrative opportunities for agronomy. *Plant and Soil*, *362*(1–2), 389–417. https://doi.org/10.1007/s11104-012-1429-7

Hutchinson, G. E. (1961). The Paradox of the Plankton. *The American Naturalist*, *95*(882), 137–145. https://doi.org/10.1086/282171

Jones, M. E., Nico, P. S., Ying, S., Regier, T., Thieme, J., & Keiluweit, M. (2018). Manganese-Driven Carbon Oxidation at Oxic–Anoxic Interfaces. *Environmental Science & Technology*, *52*(21), 12349–12357. https://doi.org/10.1021/acs.est.8b03791

Kutsch, W., Bahn, M., & Heinemeyer, A. (2009). *Soil Carbon Dynamics* (W. L. Kutsch, M. Bahn, & A. Heinemeyer, Eds.). Cambridge University Press. https://doi.org/10.1017/CBO9780511711794

Laio, F., Porporato, A., Ridolfi, L., & Rodriguez-Iturbe, I. (2001). Plants in water-controlled ecosystems: active role in hydrologic processes and response to water stress. *Advances in Water Resources*, *24*(7), 707–723. https://doi.org/10.1016/S0309-1708(01)00005-7

Li, H., Santos, F., Butler, K., & Herndon, E. (2021). A Critical Review on the Multiple Roles of Manganese in Stabilizing and Destabilizing Soil Organic Matter. *Environmental Science & Technology*, *55*(18), 12136–12152. https://doi.org/10.1021/acs.est.1c00299

Lin, W. C., Coppi, M. V., & Lovley, D. R. (2004). Geobacter sulfurreducens Can Grow with Oxygen as a Terminal Electron Acceptor. *Applied and Environmental Microbiology*, *70*(4), 2525–2528. https://doi.org/10.1128/AEM.70.4.2525-2528.2004

Liptzin, D., Silver, W. L., & Detto, M. (2011). Temporal Dynamics in Soil Oxygen and Greenhouse Gases in Two Humid Tropical Forests. *Ecosystems*, *14*(2), 171–182. https://doi.org/10.1007/s10021-010-9402-x

Lladó, S., López-Mondéjar, R., & Baldrian, P. (2017). Forest Soil Bacteria: Diversity, Involvement in Ecosystem Processes, and Response to Global Change. *Microbiology and Molecular Biology Reviews*, *81*(2). https://doi.org/10.1128/MMBR.00063-16

Lovley, D. R., Giovannoni, S. J., White, D. C., Champine, J. E., Phillips, E. J. P., Gorby, Y. A., & Goodwin, S. (1993). Geobacter metallireducens gen. nov. sp. nov., a microorganism capable of coupling the complete oxidation of organic compounds to the reduction of iron and other metals. *Archives of Microbiology*, *159*(4), 336–344. https://doi.org/10.1007/BF00290916

Ma, L., Guo, C., Lü, X., Yuan, S., & Wang, R. (2015). Soil moisture and land use are major determinants of soil microbial community composition and biomass at a regional scale in northeastern China. *Biogeosciences*, *12*(8), 2585–2596. https://doi.org/10.5194/bg-12-2585-2015

Manzoni, S., & Porporato, A. (2007). A theoretical analysis of nonlinearities and feedbacks in soil carbon and nitrogen cycles. *Soil Biology and Biochemistry*, *39*(7), 1542–1556. https://doi.org/10.1016/j.soilbio.2007.01.006

Masscheleyn, P. H., DeLaune, R. D., & Patrick, W. H. (1993). Methane and nitrous oxide emissions from laboratory measurements of rice soil suspension: Effect of soil oxidation-reduction status. *Chemosphere*, *26*(1–4), 251–260. https://doi.org/10.1016/0045-6535(93)90426-6

McLean, M. A., & Huhta, V. (2000). Temporal and spatial fluctuations in moisture affect humus microfungal community structure in microcosms. *Biology and Fertility of Soils*, *32*(2), 114–119. https://doi.org/10.1007/s003740000225

Meixner, F. X., & Yang, W. X. (2006). Biogenic emissions of nitric oxide and nitrous oxide from arid and semi-arid land. In *Dryland Ecohydrology* (pp. 233–255). Kluwer Academic Publishers. https://doi.org/10.1007/1-4020-4260-4_14

Miele, F., Benettin, P., Wang, S., Retti, I., Asadollahi, M., Frutschi, M., Mohanty, B., Bernier-Latmani, R., & Rinaldo, A. (2023). Spatially Explicit Linkages Between Redox Potential Cycles and Soil Moisture Fluctuations. *Water Resources Research*, *59*(3). https://doi.org/10.1029/2022WR032328

Mittelbach H. (2011). *Soil Moisture in Switzerland: Analyses from the Swiss Soil Moisture Experiment*. Swiss Federal Institute of Technology in Zurich.

Oertel, C., Matschullat, J., Zurba, K., Zimmermann, F., & Erasmi, S. (2016). Greenhouse gas emissions from soils—A review. *Geochemistry*, *76*(3), 327–352. https://doi.org/10.1016/j.chemer.2016.04.002

Peralta, A. L., Ludmer, S., & Kent, A. D. (2013). Hydrologic history influences microbial community composition and nitrogen cycling under experimental drying/wetting treatments. *Soil Biology and Biochemistry*, *66*, 29–37. https://doi.org/10.1016/j.soilbio.2013.06.019

Peralta, A. L., Ludmer, S., Matthews, J. W., & Kent, A. D. (2014). Bacterial community response to changes in soil redox potential along a moisture gradient in restored wetlands. *Ecological Engineering*, *73*, 246–253. https://doi.org/10.1016/j.ecoleng.2014.09.047

Pett-Ridge, J., & Firestone, M. K. (2005). Redox Fluctuation Structures Microbial Communities in a Wet Tropical Soil. *Applied and Environmental Microbiology*, *71*(11), 6998–7007. https://doi.org/10.1128/AEM.71.11.6998-7007.2005

Reeburgh, W. S. (1983). Rates of biogeochemical processes in anoxic sediments. *Annual Review of Earth and Planetary Sciences*, *11*(1), 269–298. https://doi.org/10.1146/annurev.ea.11.050183.001413

Rezanezhad, F., Couture, R.-M., Kovac, R., O'Connell, D., & Van Cappellen, P. (2014). Water table fluctuations and soil biogeochemistry: An experimental approach using an automated soil column system. *Journal of Hydrology*, *509*, 245–256. https://doi.org/10.1016/j.jhydrol.2013.11.036

Robertson, W. J., Bowman, J. P., Franzmann, P. D., & Mee, B. J. (2001). Desulfosporosinus meridiei sp. nov., a spore-forming sulfate-reducing bacterium isolated from gasolene-contaminated groundwater. *International Journal of Systematic and Evolutionary Microbiology*, *51*(1), 133–140. https://doi.org/10.1099/00207713-51-1-133

Rodríguez-Escales, P., Barba, C., Sanchez-Vila, X., Jacques, D., & Folch, A. (2020). Coupling Flow, Heat, and Reactive Transport Modeling to Reproduce *In Situ* Redox Potential Evolution: Application to an Infiltration Pond. *Environmental Science & Technology*, *54*(19), 12092–12101. https://doi.org/10.1021/acs.est.0c03056

Rodriguez-Iturbe, I., David Roxbee Cox, & Valerie Isham. (1987). Some models for rainfall based on stochastic point processes. *Proceedings of the Royal Society of London. A. Mathematical and Physical Sciences*, *410*(1839), 269–288. https://doi.org/10.1098/rspa.1987.0039

Rodriguez-Iturbe, I., Porporato, A., Ridolfi, L., Isham, V., & Coxi, D. R. (1999). Probabilistic modelling of water balance at a point: the role of climate, soil and vegetation. *Proceedings of the Royal Society of London. Series A: Mathematical, Physical and Engineering Sciences*, *455*(1990), 3789–3805. https://doi.org/10.1098/rspa.1999.0477

Ronen, D., Scher, H., & Blunt, M. (2000). Field observations of a capillary fringe before and after a rainy season. *Journal of Contaminant Hydrology*, *44*(2), 103–118. https://doi.org/10.1016/S0169-7722(00)00096-6

Rubol, S., Manzoni, S., Bellin, A., & Porporato, A. (2013). Modeling soil moisture and oxygen effects on soil biogeochemical cycles including dissimilatory nitrate reduction to ammonium (DNRA). *Advances in Water Resources*, *62*, 106–124. https://doi.org/10.1016/j.advwatres.2013.09.016

Rühle, F. A., von Netzer, F., Lueders, T., & Stumpp, C. (2015). Response of Transport Parameters and Sediment Microbiota to Water Table Fluctuations in Laboratory Columns. *Vadose Zone Journal*, *14*(5), 1–12. https://doi.org/10.2136/vzj2014.09.0116

Saltveit, M. E. (2019). Respiratory Metabolism. In *Postharvest Physiology and Biochemistry of Fruits and Vegetables* (pp. 73–91). Elsevier. https://doi.org/10.1016/B978-0-12-813278-4.00004-X

Schaefer, H., Fletcher, S. E. M., Veidt, C., Lassey, K. R., Brailsford, G. W., Bromley, T. M., Dlugokencky, E. J., Michel, S. E., Miller, J. B., Levin, I., Lowe, D. C., Martin, R. J., Vaughn, B. H., & White, J. W. C. (2016). A 21st-century shift from fossil-fuel to biogenic methane emissions indicated by 13CH4. *Science*, *352*(6281), 80–84. https://doi.org/10.1126/science.aad2705

Serrano-Silva, N., Sarria-Guzm´an, Y., Guzm´an, G., Dendooven, L., & Luna-Guido, M. (2014). Methanogenesis and Methanotrophy in Soil: A Review. In *Pedosphere* (Vol. 24, Issue 3).

Silver, W. L., Liptzin, D., & Almaraz, M. (2013). Soil redox dynamics and biogeochemistry along a tropical elevation gradient. *Bulletins*, *54*, 195–210. https://doi.org/10.2307/26796814

Silver, W. L., Lugo, A. E., & Keller, M. (1999). Soil oxygen availability and biogeochemistry along rainfall and topographic gradients in upland wet tropical forest soils. *Biogeochemistry*, *44*(3), 301–328. https://doi.org/10.1007/BF00996995

Song, Y., Deng, S. P., Acosta-Martínez, V., & Katsalirou, E. (2008). Characterization of redox-related soil microbial communities along a river floodplain continuum by fatty acid methyl ester (FAME) and 16S rRNA genes. *Applied Soil Ecology*, *40*(3), 499–509. https://doi.org/10.1016/j.apsoil.2008.07.005

Sorensen, T. A. (1948). A method of establishing groups of equal amplitude in plant sociology based on similarity of species content and its application to analyses of the vegetation on Danish commons. *Biol. Skar.*, *5*, 1–34.

Šťovíček, A., Kim, M., Or, D., & Gillor, O. (2017). Microbial community response to hydration-desiccation cycles in desert soil. *Scientific Reports*, *7*(1), 45735. https://doi.org/10.1038/srep45735

Syakila, A., & Kroeze, C. (2011). The global nitrous oxide budget revisited. *Greenhouse Gas Measurement and Management*, *1*(1), 17–26. https://doi.org/10.3763/ghgmm.2010.0007

Tecon, R., & Or, D. (2017). Biophysical processes supporting the diversity of microbial life in soil. *FEMS Microbiology Reviews*, *41*(5), 599–623. https://doi.org/10.1093/femsre/fux039

Wang, J., Bogena, H. R., Vereecken, H., & Brüggemann, N. (2018). Characterizing Redox Potential Effects on Greenhouse Gas Emissions Induced by Water-Level Changes. *Vadose Zone Journal*, *17*(1), 1–13. https://doi.org/10.2136/vzj2017.08.0152

Xiang, S.-R., Doyle, A., Holden, P. A., & Schimel, J. P. (2008). Drying and rewetting effects on C and N mineralization and microbial activity in surface and subsurface California grassland soils. *Soil Biology and Biochemistry*, *40*(9), 2281–2289. https://doi.org/10.1016/j.soilbio.2008.05.004

Yu, K., Böhme, F., Rinklebe, J., Neue, H.-U., & DeLaune, R. D. (2007). Major Biogeochemical Processes in Soils-A Microcosm Incubation from Reducing to Oxidizing Conditions. *Soil Science Society of America Journal*, *71*(4), 1406–1417. https://doi.org/10.2136/sssaj2006.0155

Zhang, Z., & Furman, A. (2021). Soil redox dynamics under dynamic hydrologic regimes - A review. In *Science of the Total Environment* (Vol. 763). Elsevier B.V. https://doi.org/10.1016/j.scitotenv.2020.143026

Zhou, X., Fornara, D., Ikenaga, M., Akagi, I., Zhang, R., & Jia, Z. (2016). The Resilience of Microbial Community under Drying and Rewetting Cycles of Three Forest Soils. *Frontiers in Microbiology*, *7*. https://doi.org/10.3389/fmicb.2016.01101